OXFORD

Cerebral Cortex, 2016; 1–16

doi: 10.1093/cercor/bhw318
Original Article

ORIGINAL ARTICLE

Trajectory of Parvalbumin Cell Impairment and Loss of Cortical Inhibition in Traumatic Brain Injury

Tsung-Hsun Hsieh[1,2,3,†], Henry Hing Cheong Lee[4,†], Mustafa Qadir Hameed[1,4,5], Alvaro Pascual-Leone[6], Takao K. Hensch[4,7] and Alexander Rotenberg[1,4,6]

[1]Neuromodulation Program, Division of Epilepsy and Clinical Neurophysiology, Department of Neurology, Boston Children's Hospital, Harvard Medical School, Boston, MA 02115, USA, [2]Department of Physical Therapy and Graduate Institute of Rehabilitation Science, College of Medicine, Chang Gung University, Taoyuan 33302, Taiwan, [3]Neuroscience Research Center, Chang Gung Memorial Hospital, Linkou Medical Center, Taoyuan 33305, Taiwan, [4]Department of Neurology, F.M. Kirby Neurobiology Center, Boston Children's Hospital, Harvard Medical School, Boston, MA 02115, USA, [5]Department of Neurosurgery, Boston Children's Hospital, Harvard Medical School, Boston, MA 02115, USA, [6]Berenson-Allen Center for Noninvasive Brain Stimulation, Beth Israel Deaconess Medical Center, Harvard Medical School, Boston, MA 02115, USA and [7]Department of Molecular and Cellular Biology, Center for Brain Science, Harvard University, MA 02138, USA

Address correspondence to Alexander Rotenberg; Takao K. Hensch, Department of Neurology, Boston Children's Hospital, 300 Longwood Avenue, Boston, MA 02115, USA. E-mail: alexander.rotenberg@childrens.harvard.edu, takao.hensch@childrens.harvard.edu

[†]T.H.H. and H.H.C.L. contributed equally to this work

Abstract

Many neuropsychiatric symptoms that follow traumatic brain injury (TBI), including mood disorders, sleep disturbance, chronic pain, and posttraumatic epilepsy (PTE) are attributable to compromised cortical inhibition. However, the temporal trajectory of cortical inhibition loss and its underlying mechanisms are not known. Using paired-pulse transcranial magnetic stimulation (ppTMS) and immunohistochemistry, we tracked functional and cellular changes of cortical inhibitory network elements after fluid-percussion injury (FPI) in rats. ppTMS revealed a progressive loss of cortical inhibition as early as 2 weeks after FPI. This profile paralleled the increasing levels of cortical oxidative stress, which was accompanied by a gradual loss of parvalbumin (PV) immunoreactivity in perilesional cortex. Preceding the PV loss, we identified a degradation of the perineuronal net (PNN)—a specialized extracellular structure enwrapping cortical PV-positive (PV+) inhibitory interneurons which binds the PV+ cell maintenance factor, Otx2. The trajectory of these impairments underlies the reduced inhibitory tone, which can contribute to posttraumatic neurological conditions, such as PTE. Taken together, our results highlight the use of ppTMS as a biomarker to track the course of cortical inhibitory dysfunction post-TBI. Moreover, the neuroprotective role of PNNs on PV+ cell function suggests antioxidant treatment or Otx2 enhancement as a promising prophylaxis for post-TBI symptoms.

Key words: intracortical inhibition, Otx2, oxidative stress, perineuronal nets, transcranial magnetic stimulation

Introduction

Traumatic brain injury (TBI) results in a range of neurologic symptoms, such as chronic pain (Andary et al. 1997), mood disorders (Jorge et al. 2007), sleep disturbance (Hou et al. 2013), increased seizure susceptibility (Golarai et al. 2001), and posttraumatic epilepsy (PTE) (Lucke-Wold et al. 2015), which are referable to compromised cortical inhibition. Notably, posttraumatic neurologic symptoms often do not immediately follow TBI. Rather, as most apparent in PTE and posttraumatic epileptogenesis, many such symptoms follow an asymptomatic post-TBI latent period of weeks to months (Jensen 2009; Lowenstein 2009; Valk-Kleibeuker et al. 2014; Sawyer et al. 2015; Theadom et al. 2015). Presumably, cortical inhibition is lost during the latent post-TBI period. Yet the molecular and cellular mechanisms underlying this TBI pathophysiology are poorly understood, thus leading to difficulty in prophylactic treatment of prevalent posttraumatic syndromes (Nampiaparampil 2008; Prince et al. 2009; Rakhade and Jensen 2009; Torbic et al. 2013; Jorge and Arciniegas 2014; Rao et al. 2014; Lefebvre et al. 2015; Major et al. 2015).

Previous studies indicate that the pathologic shift of cortical excitatory:inhibitory (E:I) ratio toward excess excitation after TBI is primarily due to loss of synaptic inhibition mediated by γ-aminobutyric acid (GABA) and a reduction of GABA-synthesizing enzymes in inhibitory synapses in the neocortex (Prince and Jacobs 1998; Huusko and Pitkanen 2014; Cantu et al. 2015). However, evidence of such loss of inhibitory tone in vivo is lacking. Thus, we applied paired-pulse transcranial magnetic stimulation (ppTMS) to test whether GABA-mediated cortical inhibition is reduced after TBI in vivo in a rat fluid percussion injury (FPI) model (Hunt et al. 2013).

In ppTMS, intracranial stimulating currents delivered as paired pulses are generated by a powerful and fluctuating extracranial magnetic field. Most commonly, ppTMS is applied to the motor cortex to elicit a quantifiable motor response whose suppression or facilitation can be used to characterize the cortical *E:I* ratio (Barker et al. 1984; Kobayashi and Pascual-Leone 2003; Ziemann et al. 2015). One ppTMS protocol in particular, where the paired stimuli are separated by a 50–250 ms interval termed long-interval ppTMS (LI-ppTMS), has been applied extensively to measure intracortical inhibition (known as long-interval cortical inhibition, LICI) in patients with epilepsy and related disorders of impaired cortical inhibition (Bashir et al. 2012; Badawy et al. 2014).

We recently adapted LI-ppTMS to rats, and found that the magnitude of paired-pulse inhibition of the motor-evoked response reflects cortical $GABA_A$ receptor-mediated inhibition (Vahabzadeh-Hagh et al. 2011; Hsieh et al. 2012). In this report, as a step toward translation of preclinical LI-ppTMS to applications in human neurologic syndromes, we tested whether loss of cortical inhibition after TBI in rats is reflected in ppTMS metrics of cortical inhibition. Specifically, as rat FPI reliably causes PTE and other posttraumatic syndromes several weeks after injury (D'Ambrosio et al. 2005; Sun et al. 2008; Shultz et al. 2012; Goodrich et al. 2013; Hameed et al. 2014; Rowe et al. 2014; Skopin et al. 2015), we tested whether loss of LICI can be detected by LI-ppTMS within the subacute post-TBI period in the FPI model.

To further delineate the temporal course of post-TBI loss of cortical inhibition, we also performed complementary studies aimed at characterizing posttraumatic changes in cortical GABAergic interneurons (Cantu et al. 2015). We focused on the parvalbumin positive (PV+) cells that comprise the majority of cortical GABA circuitry (Rudy et al. 2011; Kelsom and Lu 2013) and are particularly vulnerable to metabolic challenges after injury due to their baseline fast-firing rate and high metabolic demand (Andre et al. 2001). PV+ cells are enwrapped by a specialized extracellular structure known as the perineuronal net (PNN) which protects them from oxidative stress and is crucial to sustain PV+ cell viability and function, particularly after brain injury (Sugiyama et al. 2009; Carulli et al. 2010; Cabungcal et al. 2013b; Rodriguez-Rodriguez et al. 2014). Importantly, PV+ cell inhibitory capacity depends on PNN integrity (Kwok et al. 2011). We previously showed that Otx2, a homeoprotein found in cortical PV+ cells, binds preferably to disulfated N-acetylgalactosamine units in the PNN glycosaminoglycan sidechains, and such Otx2 binding is critical for PV+ cell survival (Beurdeley et al. 2012). To test whether and how PV+ cell impairment underlies any posttraumatic inhibitory loss (Petronilho et al. 2010), we examined the relative temporal trajectory of these molecular entities (PV+ cell count, oxidative stress level, PNN integrity, and Otx2 accumulation) after FPI (Greve and Zink 2009; Pitkanen et al. 2009).

We report that LI-ppTMS detects early impairment of cortical inhibition after TBI, and that such loss of inhibitory tone correlates with a progressive PV+ cell loss. Our data also indicate that sustained oxidative stress, in parallel to Otx2 depletion and PNN loss in the cortex, contributes to posttraumatic cortical pathophysiology, and raises prospects for mitigating PV+ cell vulnerability after TBI with antioxidant treatment or Otx2 replacement (Fraser and Morrison 2009). Given the mechanistic similarity between human and rat LI-ppTMS (Hsieh et al. 2012; Vahabzadeh-Hagh et al. 2012), we expect that these neurobiological insights into the post-TBI loss of cortical inhibition will provide valuable opportunities for translation to humans.

Materials and Methods

Animal Preparation

Experiments were performed on adult male Long-Evans rats (250–300 g). Rats were housed in standard cages in a temperature-controlled facility with a 12-h light/dark cycle and a continuous supply of water and food ad libitum. All animal procedures were approved by the Institutional Animal Care and Use Committee (IACUC) at Boston Children's Hospital and in accordance with the National Institutes of Health (NIH) Guide for the Care and Use of Laboratory Animals.

Fluid Percussion Injury

Rats were anesthetized with 2–4% isoflurane vapor (Baxter Pharmaceutical) and their heads secured in a stereotaxic frame. The level of anesthesia was carefully monitored via heart rate and breathing rate such that it was maintained constant throughout the surgical procedure. Rats were monitored for immediate post-TBI apnea, and were discarded from the experiment if duration of apnea was >30 s. A unilateral circular craniotomy centered 2 mm posterior to bregma (bregma −2 mm) and 2 mm lateral to the mid-ridge (mid-ridge +2 mm) was made over the left convexity. The anterior and lateral edges of the craniotomy were adjacent to the coronal suture and left lateral ridge, respectively. TBI was induced using a fluid-percussion device (AmScien Instruments) (Hameed et al. 2014). In the verum experimental TBI group, a fluid percussion wave of 2.0–2.5 atm was delivered against the exposed intact dura. Pressure pulses were measured by a transducer extracranially and recorded on a storage oscilloscope. Sham control TBI animals underwent the same surgical procedures, but did not receive FPI.

Previously, we and others reported that approximately 100% of rats receiving this and similar forms of FPI developed recurrent late posttraumatic seizures, 6–12 weeks after injury (D'Ambrosio et al. 2005; Goodrich et al. 2013), in addition to a variety of posttraumatic sequelae including ectopic gene expressions (Hayes et al. 1995), anxiety-like behavior (Rodgers et al. 2012), and ataxia (Potts et al. 2009) which could be associated with impaired neuronal inhibition (Guerriero et al. 2015).

Paired-Pulse Transcranial Magnetic Stimulation

For LI-ppTMS measures of cortical inhibition in conscious rats, we employed our previously established protocol for coupling ppTMS with mechanomyography (MMG), a non-invasive measure of cortico-spinal activation in non-anesthetized rats (Hsieh et al. 2012). Rats were restrained on a platform by straps securing the head, upper, and mid-torso as previously described (Hsieh et al. 2012). Limb acceleration resultant from each successive TMS pulse was recorded using a miniature 3-axis accelerometer (AGB3V2) secured with adhesive tape to each hind limb (see Supplementary Fig. S1).

MMG output was quantified as the peak-to-peak sum of the three vectors. LI-ppTMS was administered with a figure-of-eight coil (outside lobe diameter = 66 mm, inside diameter = 15 mm; Double Small Coil, Magstim) connected to a Magstim Rapid stimulator (Magstim). The stimulating coil was positioned using a micromanipulator, with the center of the coil midline over the dorsal scalp to elicit bilateral hind limb MMG.

To accommodate a short time period, approximately 3 min, during which an immobilized rat remains relatively motionless beneath the stimulating coil, paired TMS pulses (each individual stimulus of the 2 paired stimuli was at the same intensity) were delivered over a range of progressively increasing stimulus intensities (60%, 70%, 80%, 90%, and 100% maximum machine output (MO)). Six stimulus pairs were delivered per stimulation intensity. Each pair of stimuli was 5 s apart. Thirty pairs of stimuli were delivered with interstimulus interval (ISI) of 100 ms and 30 pairs of stimuli were delivered with ISI 200 ms. The entire ppTMS procedure was repeated weekly for each rat after TBI. Results obtained with 100 ms ISI or 200 ms ISI stimuli were analyzed separately. MMG signals were digitized at 10 kHz, band-pass filtered from 1 to 250 Hz and stored for further offline analysis (PowerLab 8/30; ADInstruments). The paired-pulse inhibition ratio was calculated from each motor response pair where the TMS-evoked MMG following the conditioning stimulus exceeded baseline noise by >3 standard deviations. The calculated ratios (conditioning MMG:test MMG) were averaged across stimulus intensities per ISI for each rat at each time point as previously described (Hsieh et al. 2012).

Three separate cohorts of experimental rats were used to test 1) whether serial, weekly ppTMS for 6 weeks detects progressive cortical dysfunction post-TBI, 2) whether a single, late ppTMS at 6 weeks after injury detects cortical inhibitory dysfunction, and 3) whether cellular substrates of progressive cortical dysfunction over 6 weeks can be identified by serial, biweekly anatomical labeling.

Perfusion of Cortical Tissues and Immunostaining

As mentioned above, a separate cohort of rats previously never exposed to ppTMS was used for perfusion and immunostaining after TBI, to avoid potential confound of ppTMS affecting the molecular metrics of interest in this study (Mix et al. 2010; Benali et al. 2011). Under deep anesthesia, rats were perfused transcardially with ice-cold saline followed by 4% paraformaldehyde (PFA). Brain tissue was dissected and postfixed in 4% PFA for 2 h at room temperature before transferring into 30% sucrose. Cryopreserved brain tissue was then frozen with Tissue-Tek O.C. T. compound (Sakura Finetek) and stored at −80°C for at least 24 h before sectioning. Using a cryostat microtome (Leica CM3050 S), free-floating cryosections (coronal sections, 30 μm) were produced at −20°C, washed briefly with phosphate-buffered saline and incubated with primary antibodies (see details below) overnight at 4°C followed by Alexa Fluor-conjugated secondary antibodies for 2 h at room temperature.

We used anti-PV (rabbit polyclonal, Swant) to investigate PV-expressing interneurons. Oxidative stress levels were assessed by antibody against 8-hydroxy-2′-deoxyguanosine (anti-8-oxo-dG, mouse monoclonal, Trevigen) (Cabungcal et al. 2013b), a modified nucleoside commonly detected as a by-product of mitochondrial DNA damage. PNN integrity was studied using biotinylated *Wisteria floribunda agglutinin* (WFA) (Sigma-Aldrich), a plant lectin which binds to chondroitin sulfate proteoglycan (CSPG) chains of PNN (Carulli et al. 2007; Beurdeley et al. 2012). To measure the accumulation of Otx2 in the cortex (Spatazza et al. 2013), we used a mouse anti-Otx2 monoclonal antibody, a gift from Dr Alain Prochiantz. Neuronal counts were performed by immunostaining with anti-NeuN (mouse monoclonal, Millipore). Secondary antibodies (Invitrogen) included: anti-mouse Alexa Fluor 488, anti-mouse Alex Fluor 594, anti-rabbit Alex Fluor 594, and Alex Fluor 594-conjugated streptavidin. All perfusion, tissue fixation, and immunostaining procedures were carried out under the same conditions using the same batch of buffers to minimize variability between samples. Immunostained sections were mounted using Fluoromount medium containing 4′,6′-diamidino-2-phenylindole (DAPI) nuclear counterstain (Southern Biotechnology), and images acquired on an Olympus Fluoview FV1000 confocal microscope.

Imaging and Analysis

Regions in the motor cortex medial to the FPI site (bregma −2 mm and mid-ridge +2 mm) were first identified by fluorescence imaging under low power magnification (×10 objective). An example of injury site revealed by DAPI staining is shown in Supplementary Fig. S2. Serial coronal sections were examined to identify the lesion site which was reliably marked by gray matter atrophy, enlarged lateral ventricle, and compressed hippocampus (Hameed et al. 2014). Perilesional site was defined as approximately 100 μm medial to the edge of the lesion (Cantu et al. 2015) without apparent cortical atrophy (see Supplementary Fig. S2). Serial coronal sections through perilesional and contralesional regions (in the opposite hemisphere) were taken from each animal (N = 5 per time point) for imaging and subsequent analysis, and two sections from each animal were used for analysis per immunoreaction (i.e., PV, WFA, Otx2, 8-oxo-dG, and NeuN). Cortical layers were identified by DAPI staining and imaging area aligned such that layer I was on the top and layer VI at the bottom. Confocal images were taken under a ×20 objective (unless otherwise stated as in low power magnification, in which case a ×10 objective was used). Image acquisitions were carried out using the FV10-ASW software (version 2.1 C), with the following parameters: 5% laser output, ×1 gain control, laser intensity between 500 and 700, offset between 10% and 15% such that signals were within the linear range. Individual channels were acquired sequentially.

Images were analyzed by ImageJ software as described previously (Beurdeley et al. 2012; Spatazza et al. 2013). First,

regions corresponding to layers II–VI, 400 μm wide in the middle of the imaging field (primary motor area coordinates above) were chosen. Then, by setting the same threshold for all images, and applying filters for size (50–5000 μm^2) and circularity (0–1.0), cells positively stained for PV, Otx2, NeuN, and WFA were identified above background signals (see Supplementary Fig. S3). DAPI counterstain was further used to visually confirm that all counted structures are cells. The number of cells identified above and 8-oxo-dG signal intensities were then measured by the software. Results from perilesional and contralesional regions of verum TBI subjects were normalized to sham-operated controls. To further study whether these anatomical changes were limited to ipsilesional cortex, a ratio between perilesional and contralesional regions was also calculated. PNNs were stained by WFA (Fig. 5A) and the complexity of PNN branches revealed by hand-tracing (Fig. 6A) (Carulli et al. 2010).

Data Processing and Statistical Analysis

Data were analyzed using SPSS version 17.0 (SPSS Inc.) with the significance level set at $P < 0.05$. All data are presented as mean ± standard error of the mean (mean ± SEM). Paired-pulse inhibition was expressed as ratio (percentage) of the conditioned evoked MMG to unconditioned evoked MMG.

Sequential LI-ppTMS measures after TBI were compared by repeated measures analysis of variance (ANOVA), with GROUP and TIME as factors. Post hoc Fisher's least significant difference (LSD) tests were used to compare means at individual time points. LI-ppTMS metrics obtained from a separate rat cohort that was not exposed to TMS except at a single time point, 6 weeks after TBI, were averaged, and compared by unpaired t-test.

Immunostaining comparisons between rats in the verum or sham TBI groups were performed by one-way ANOVA with Tukey's multiple comparison post hoc test. Immunostaining data are expressed as % Sham values. Ratios of perilesional and contralesional sides were also compared between verum TBI animals and sham-operated controls (expressed as % Sham).

Results

LI-ppTMS Reveals Posttraumatic Loss of Intracortical Inhibition

Following TBI, LI-ppTMS revealed progressive loss of paired-pulse intracortical inhibition as a function of time in injured rats

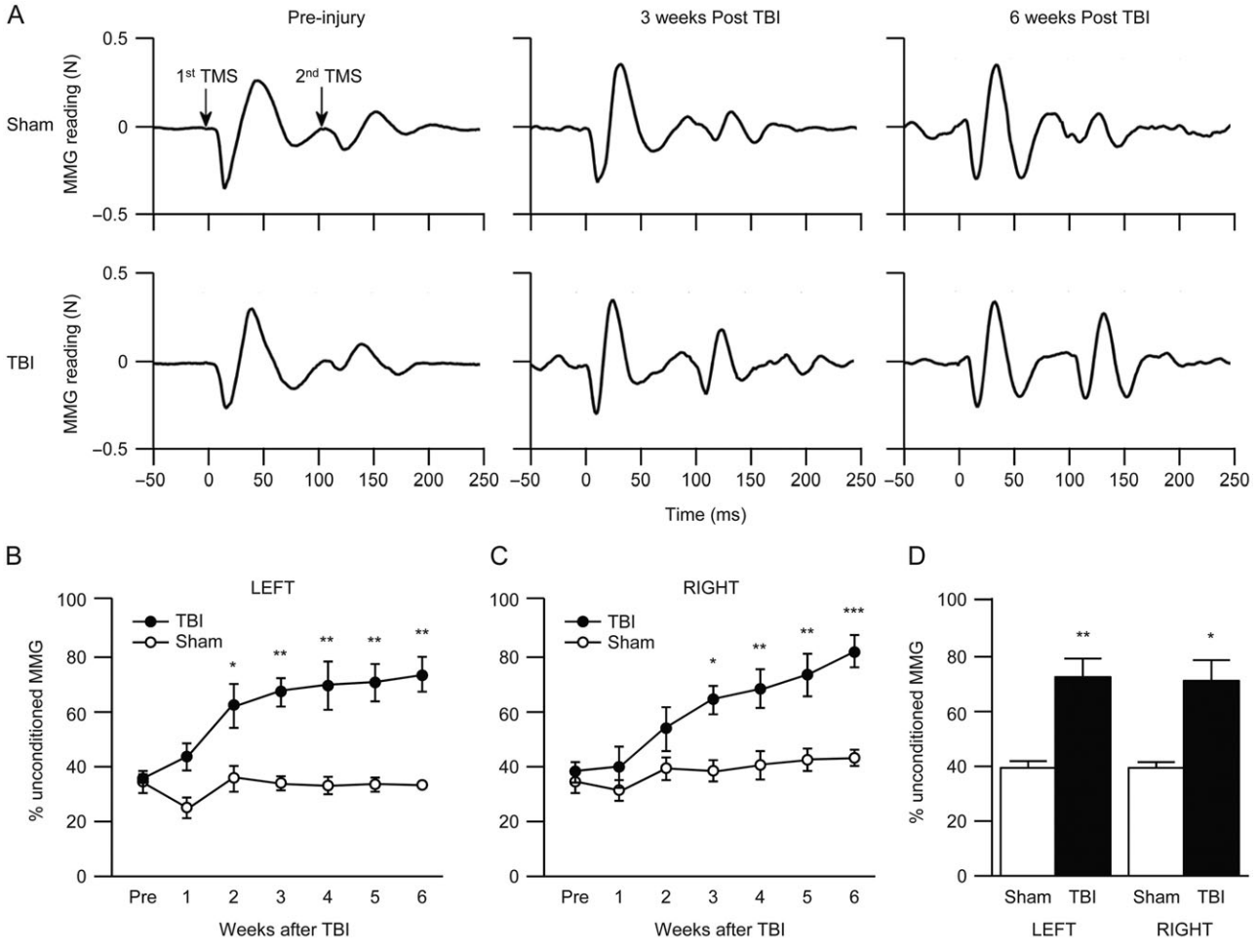

Figure 1. LI-ppTMS reveals progressive loss of intracortical inhibition following TBI. (*A*) Representative MMG traces with 100 ms ISI with 100% MO intensity show no obvious changes between pre- and post-injury (3 and 6 weeks) in the sham control (upper panel, left to right) but progressive reduction in inhibition after TBI (lower panel, left to right). (*B*, *C*) Time course of LI-ppTMS changes at 100 ms ISI in left limb (*B*, closed circle •) and right limb (*C*, closed circle •) of TBI rats ($N = 6$). Sham control groups are shown in both panels as open circle (o) ($N = 5$). Error bars = SEM, *$P < 0.05$, **$P < 0.01$, ***$P < 0.001$ Fisher LSD. (*D*) Average paired-pulse inhibition (also with 100 ms ISI) in a separate cohort of rats tested 6 weeks after verum or sham TBI. To control for the confound of weekly stimulation, these groups were not exposed to ppTMS until 6 weeks after injury (error bars = SEM, *$P < 0.05$, **$P < 0.01$, **$P < 0.001$, unpaired t-test, $N = 5$ per group).

(Fig. 1A), both relative to the sham TBI condition and relative to the pre-TBI baseline. Repeated measures ANOVA identified significant main effects of TIME ($F_{6,54} = 6.29$, $P < 0.001$ in left limb; $F_{6,54} = 6.20$, $P < 0.001$ in right limb) and INJURY ($F_{1,9} = 16.66$, $P = 0.003$ in left limb; $F_{1,9} = 18.65$, $P = 0.002$ in right limb), but no significant TIME × INJURY interaction ($F_{6,54} = 1.46$, $P = 0.21$ in left limb; $F_{6,54} = 1.40$, $P = 0.23$ in right limb).

Relative to pre-TBI baseline, post hoc analyses identified that inhibition was significantly decreased from 2 weeks onward post-TBI ($P < 0.01$) as measured in the left limb, and from 3 weeks onward post-TBI ($P < 0.01$) as measured in the right limb (Fig. 1B, C). Importantly, no significant LI-ppTMS inhibition change was detected throughout the 6-week testing duration in the sham TBI group, supporting the hypothesis that cortical inhibition was specifically impaired after injury. Similar results were also found after interrogation by LI-ppTMS with 200 ms ISI (see Supplementary Fig. 4).

To control for the potential confound of repeated, weekly stimulation which may affect cortical excitability (Muller et al. 2014), a separate cohort of rats underwent verum or sham FPI ($N = 5$ per group), was housed in their home cages without further intervention, and was tested by ppTMS 6 weeks after injury. Figure 1D shows changes in LI-ppTMS inhibition in this cohort where *t*-tests revealed a significant effect of group in left hind limb ($t = 3.83$, $P = 0.003$) and right hind limb ($t = 3.06$, $P = 0.012$) at 100ms ISI, with reduced paired-pulse inhibition in the verum-treated rats. Similar results were also found with LI-ppTMS at 200 ms ISI (see Supplementary Fig. 4). Together, our data suggest that successive sessions of ppTMS with MMG after TBI do not cause any potentiation or depression of cortical excitability.

TBI Induces Progressive Imbalance of PV+ Cells Across Hemispheres

The number of PV+ cells in the perilesional cortex was progressively reduced after injury compared with sham-operated control ($F_{5,22} = 30.93$, $P < 0.0001$) (Fig. 2A). Post hoc tests revealed significantly decreased perilesional PV+ cell numbers at all time points (2 weeks: 117 ± 6 cells/mm^2, 84 ± 4% Sham, $q = 4.812$, $P < 0.05$; 4 weeks: 99 ± 3 cells/mm^2, 71 ± 3% Sham, $q = 8.905$, $P < 0.001$; 6 weeks: 81 ± 3 cells/mm^2, 53 ± 1% Sham, $q = 12.88$, $P < 0.001$) (Fig. 2B). By comparison, in the contralesional hemisphere, there was no significant loss of cortical PV+ cells until 6 weeks post-TBI ($F_{5,22} = 0.33$, $P = 0.89$), suggesting a different trajectory of PV+ cell loss across hemispheres after TBI. To verify this, the perilesional:contralesional cortical PV+ cell ratio revealed a gradually emerging inter-hemispheric PV+ cell imbalance starting 4 weeks post-TBI ($P < 0.032$) and onward to 6 weeks ($P < 0.029$).

TBI Induces Delayed Oxidative Stress in the Cortex

Next, we asked whether progressive PV+ cell loss might reflect their vulnerability to oxidative stress (Cabungcal et al. 2013b), a

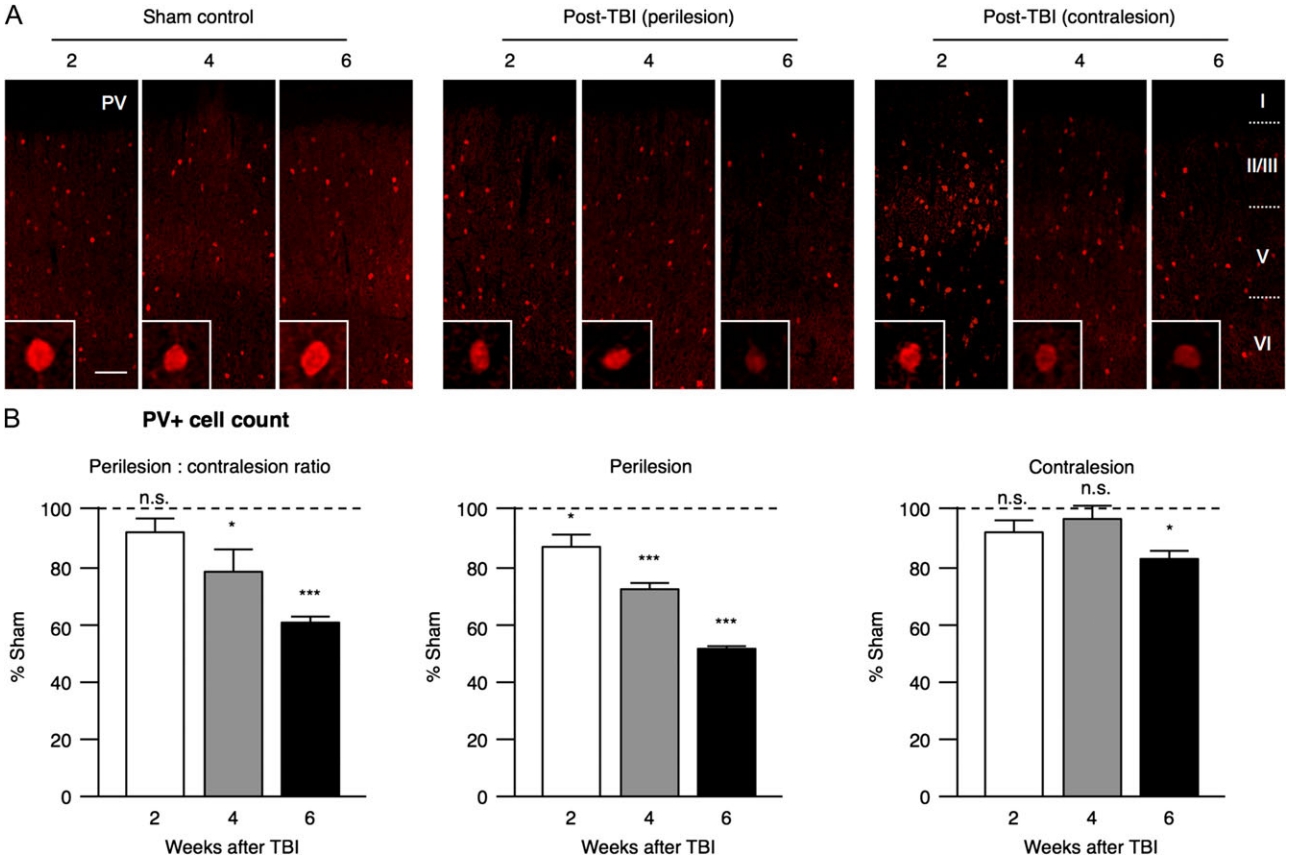

Figure 2. PV+ cell loss after TBI. (A) Rats underwent sham operation (Sham) or FPI (post-TBI) then sacrificed at different time points (2, 4, and 6 weeks). Cortical sections through motor area were immunostained with antibodies against PV (anti-PV, Swant). Confocal images (900 × 400 μm) from Sham control, perilesional and contralesional sides from post-TBI brains are shown. Cortical layers I–VI are indicated. Scale bar = 100 μm. High magnification images of individual cells are displayed in insets. (B) The number of PV+ cells at the perilesional side (middle panel), contralesional side (right panel), and their ratio (left panel) calculated for each time point after TBI (2, 4, and 6 weeks) (error bars = SEM, n.s. = not significant, *$P < 0.05$, **$P < 0.01$, ***$P < 0.001$, Tukey's multiple comparison test, $N = 5$ per group).

common consequence after TBI (Awasthi et al. 1997). As shown in Figure 3A, immunostaining for mitochondrial DNA damage with 8-oxo-dG markedly increases in intensity only at 4 and 6 weeks, but not at 2 weeks post-TBI. In perilesional regions, a progressive change emerged after injury ($F_{5,22}$ = 31.88, $P < 0.0001$) and post hoc tests revealed significant differences between sham and verum TBI starting at 4 weeks (259 ± 20% Sham, q = 13.28, $P < 0.001$) and onward to 6 weeks (216 ± 13% Sham, q = 8.62, $P < 0.001$) (Fig. 3B). On the contralesional side, there was also an overall effect of injury on 8-oxo-dG staining ($F_{5,22}$ = 3.458, $P < 0.05$), but post hoc testing did not show a significant difference between groups at individual time points. Similar to PV+ cell counts, the perilesional:contralesional ratio revealed significant redox imbalance across hemispheres only after 4 weeks post-TBI (q = 10.03, $P < 0.001$) and onward to 6 weeks (q = 5.504, $P < 0.01$; post hoc Tukey's Multiple Comparison Test), indicating a progressive build-up of oxidative stress across hemispheres post-TBI.

To determine whether this delayed oxidative stress after severe TBI has a global impact on cortical architecture, immunostaining for NeuN was performed (Fig. 4A). In contrast to changes in the number of PV+ cells, the number of NeuN+ cells over time after TBI remained unaltered in both perilesional ($F_{5,22}$ = 0.1511, P = 0.9775; 2 weeks: 1260 ± 108 cells/mm^2, 95 ± 8% Sham, q = 0.9175, $P > 0.05$, 4 weeks: 1344 ± 93 cells/mm^2, 101 ± 7% Sham, q = 0.1433, $P > 0.05$, 6 weeks: 1455 ± 60 cells/mm^2, 98 ± 4% Sham, q = 0.2889, $P > 0.05$) and contralesional regions ($F_{5,22}$ = 0.23, P = 0.9453; 2 weeks: 1326 ± 102 cells/mm^2, 102 ± 8% Sham, q = 0.3462, $P > 0.05$, 4 weeks: 1320 ± 18 cells/mm^2, 101 ± 1% Sham, q = 0.1064, $P > 0.05$, 6 weeks: 1407 ± 39 cells/mm^2, 94 ± 3% Sham, q = 1.029, $P > 0.05$) (Fig. 4B).

Quantification of layer V thickness as one metric was not significantly altered in perilesional ($F_{5,22}$ = 0.3559, P = 0.8729; 2 weeks: 99 ± 5% Sham, q = 0.1315, $P > 0.05$, 4 weeks: 106 ± 5%, q = 1.454, $P > 0.05$, 6 weeks: 101 ± 3% Sham, q = 0.1272, $P > 0.05$) or contralesional cortex ($F_{5,22}$ = 1.036, P = 0.4214; 2 weeks: 106 ± 7% Sham, q = 1.139, $P > 0.05$, 4 weeks: 115 ± 6% Sham, q = 2.572, $P > 0.05$, 6 weeks: 102 ± 4% Sham, q = 0.2999, $P > 0.05$) (Fig. 4C). Together, these data suggest that the gross cortical architecture in the perilesional region is relatively preserved in this rat FPI model.

Early PNN Degradation and Loss of Otx2 Homeoprotein

To further understand PV+ cell vulnerability to oxidative stress after TBI, we investigated the integrity of neuroprotective PNNs by WFA staining (Fig. 5A). We found a strong overall effect of injury on the number of WFA-positive (WFA+) cells in the perilesional cortex ($F_{5,22}$ = 69.88, $P < 0.0001$), in contrast to the sham control in which the number of WFA+ cells remained constant throughout. Post hoc tests revealed an early decline in WFA+

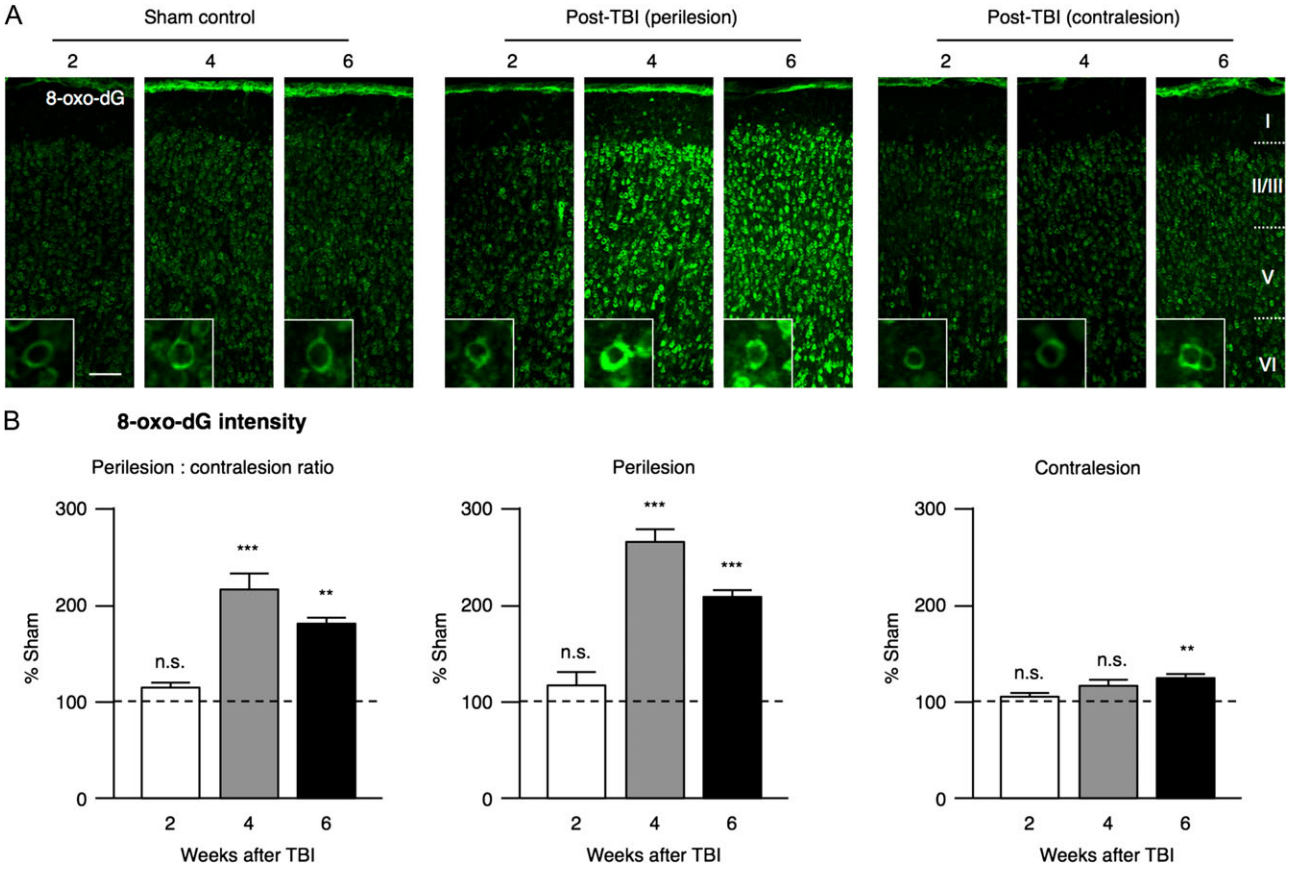

Figure 3. Increased oxidative stress after TBI. (A) Rats underwent sham operation (Sham) or FPI (post-TBI) then sacrificed at different time points (2, 4, and 6 weeks). Cortical sections through motor area were immunostained with antibodies against mitochondrial DNA damage (anti-8-oxo-dG, Trevigen). Confocal images (900 × 400 μm) from Sham control, perilesional and contralesional sides from post-TBI brains are shown. Cortical layers I–VI are indicated. Scale bar = 100 μm. High magnification images of individual cells are displayed in insets. (B) The signal intensity for 8-oxo-dG immunostaining at the perilesional side (middle panel), contralesional side (right panel), and their ratio (left panel) calculated for each time point after TBI (2, 4, and 6 weeks) (error bars = SEM, n.s. = not significant, **$P < 0.01$, ***$P < 0.001$, Tukey's multiple comparison test, N = 5 per group).

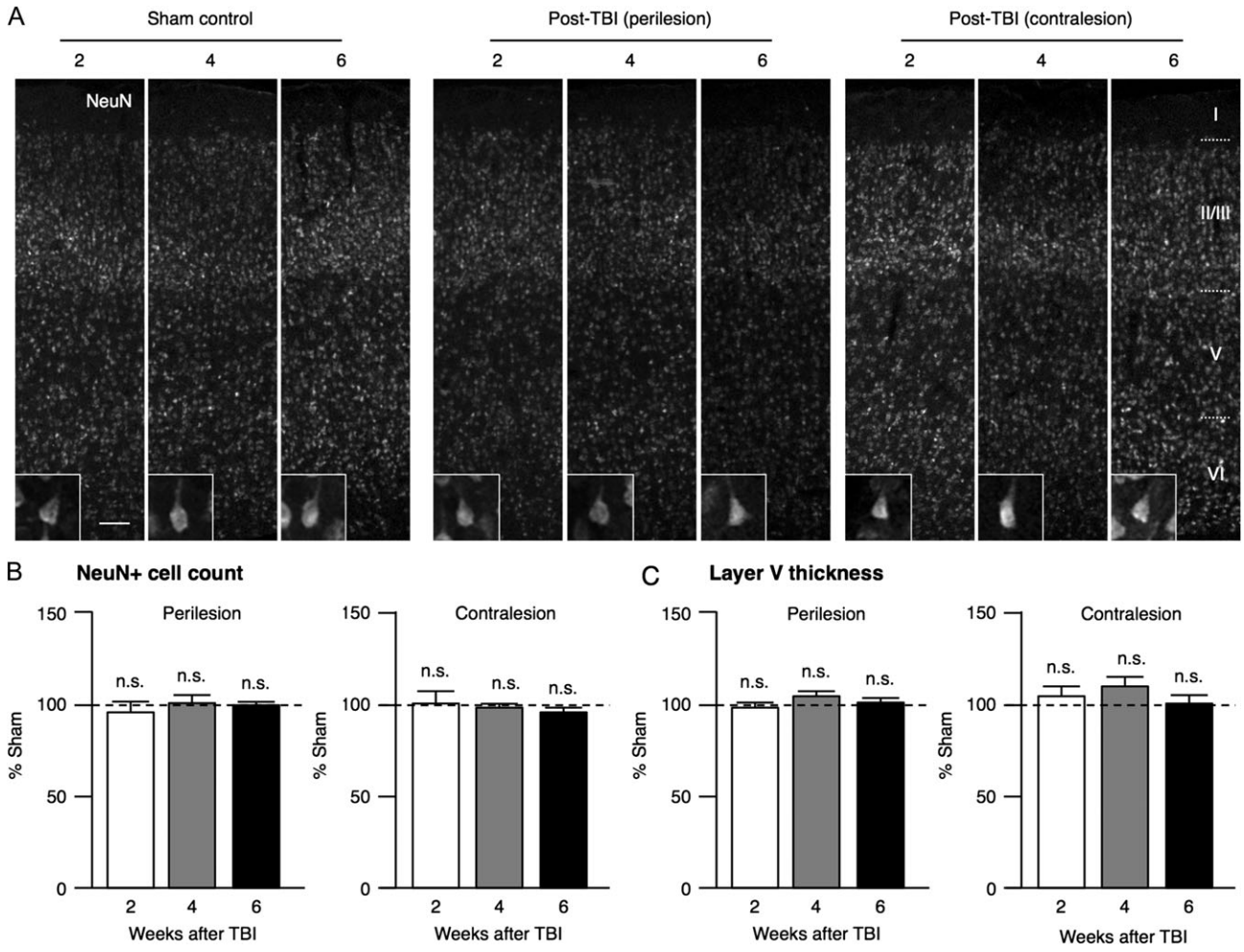

Figure 4. Unchanged neuronal cell counts and cortical thickness after TBI. (A) Rats underwent sham operation (Sham) or fluid percussion injury (post-TBI) then sacrificed at different time points (2, 4 and 6 weeks). Cortical sections through motor area were immunostained with antibodies against NeuN (anti-NeuN, Millipore). Confocal images (900 x 400μm) from Sham control, perilesional and contralesional sides from Post-TBI brains are shown. Cortical layers I-VI are indicated. Scale bar = 100 μm. High magnification images of individual cells are displayed in insets. (B) Quantification of NeuN immunostaining. The proportion of identified NeuN-positive cells at the perilesional (left panel)or contralesional sides (right panel) calculated with respect to sham for each time point after TBI (2, 4 and 6 weeks). (C) The thickness of layer V at the perilesional (left panel) or contralesional sides (right panel) calculated for each time point after TBI (2, 4 and 6 weeks). (Error bars = S.E.M., n.s. = not significant, Tukey's multiple comparison test, N = 5 per group)

cell numbers from the first post-TBI period onward (2 weeks: 60 ± 6 cells/mm^2, 62 ± 5% Sham, q = 9.21, P < 0.001; 4 weeks: 27 ± 3 cells/mm^2, 27 ± 2% Sham, q = 17.21, P < 0.001; 6 weeks: 21 ± 3 cells/mm^2, 24 ± 3% Sham, q = 16.45, P < 0.001) (Fig. 5B). There was also an overall effect of injury in the contralesional cortex ($F_{5,22}$ = 5.134, P < 0.01), with post hoc analysis showing a significant decrease in WFA+ cells 2 weeks after injury (69 ± 5 cells/mm^2, 80 ± 5% Sham, q = 4.998, P < 0.05).

Moreover, PNN tracing (Fig. 6A) revealed a significant reduction in branch number in perilesional cortex ($F_{5,294}$ = 65.27, P < 0.0001), again from the earliest time point examined and progressively dropping thereafter (2 weeks: 55 ± 4% Sham, q = 11.09, P < 0.001; 4 weeks: 41 ± 5% Sham, q = 14.32, P < 0.001; and 6 weeks: 29 ± 4% Sham, q = 17.44, P < 0.001) (Fig. 6B), in contrast to sham control. Notably, there was also a mild but significant overall effect of injury on PNN branch number in the contralesional hemisphere ($F_{5,294}$ = 25.09, P < 0.0001) at all time points (2 weeks: 66 ± 4% Sham, q = 7.586, P < 0.001; 4 weeks: 81 ± 5% Sham, q = 4.23, P < 0.001; 6 weeks: 47 ± 5% Sham, q = 12.03, P < 0.001) (Fig. 6B).

To gain further insights into the dynamics of PNN changes in PV+ cell populations, we carried out double-immunostaining for WFA and PV. There was a significant effect of injury on the percentage of PV+ cells enwrapped by PNNs in the perilesional cortex ($F_{5,54}$ = 78.42, P < 0.0001) as well as on the contralesional side ($F_{5,54}$ = 4.791, P < 0.0001). Post hoc analysis revealed a significant perilesional reduction (2 weeks: q = 12.34, P < 0.001; 4 weeks: q = 18.45, P < 0.001; 6 weeks: q = 14.81, P < 0.001), but a significant reduction only 6 weeks after TBI on the contralesional side (q = 4.321, P < 0.05) (Fig. 7B).

Interestingly, we also found an overall effect of injury on the converse percentage of WFA+ cells that are PV+ in both hemispheres (perilesional: $F_{5,54}$ = 20.24, P < 0.0001; contralesional: $F_{5,54}$ = 25.55, P < 0.0001). Post hoc analysis further revealed a reduction in the perilesional cortex throughout the 6-week post-TBI period (2 weeks: q = 9.941, P < 0.001; 4 weeks: q = 7.431, P < 0.001; 6 weeks: q = 6.609, P < 0.001) as compared with the contralesional side (6 weeks: q = 12.23, P < 0.001) (Fig. 7C).

Concomitant with PNN weakening, the number of Otx2+ cells in perilesional cortex was rapidly reduced throughout the post-TBI

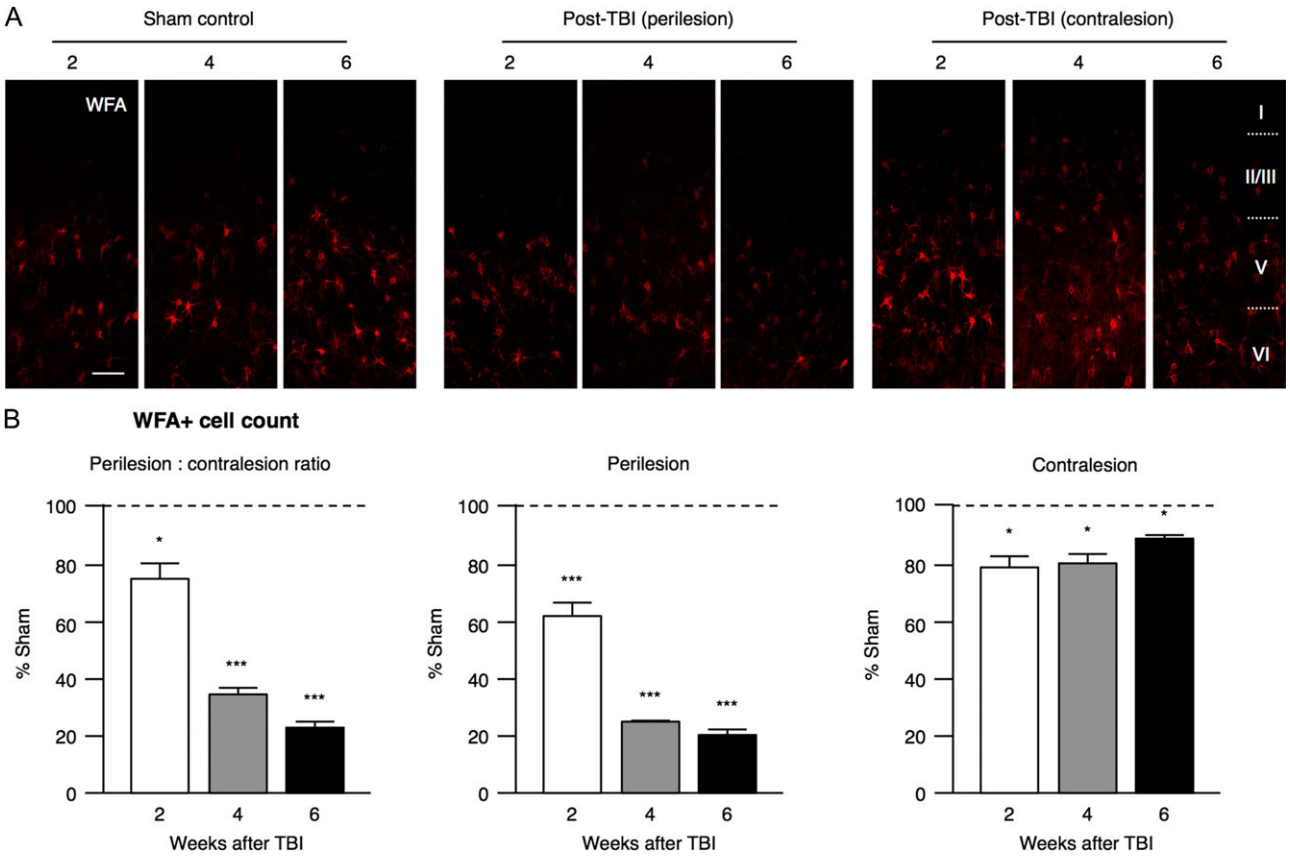

Figure 5. Reduced PNN+ cells after TBI. (A) Rats underwent sham operation (Sham) or FPI (post-TBI) then sacrificed at different time points (2, 4, and 6 weeks). Cortical sections through motor area were stained with *Wisteria floribunda agglutinin* (WFA, Sigma-Aldrich) to reveal PNN structure. Confocal images (900 × 400 μm) from Sham control, perilesional and contralesional sides from post-TBI brains are shown. Cortical layers I–VI are indicated. Scale bar = 100 μm (see Fig. 6 for high magnification images of individual cells). (B) The number of cells positively stained for WFA at the perilesional side (middle panel), contralesional side (right panel), and their ratio (left panel) calculated for each time point after TBI (2, 4, and 6 weeks) (error bars = SEM, n.s. = not significant, *$P < 0.05$, ***$P < 0.001$, Tukey's multiple comparison test, $N = 5$ per group).

period ($F_{5,22} = 40.63$, $P < 0.0001$; 2 weeks: 33 ± 3 cells/mm^2, 52 ± 2% Sham, $q = 11.41$, $P < 0.001$; 4 weeks: 30 ± 2 cells/mm^2, 46 ± 1% Sham, $q = 12.91$, $P < 0.001$; 6 weeks: 34 ± 1 cells/mm^2, 51 ± 1% Sham, $q = 10.4$, $P < 0.001$) (Fig. 8A, B). In the contralesional cortex, this loss of Otx2+ cells occurred later and to a lesser extent ($F_{5,22} = 10.09$, $P < 0.0001$; 4 weeks: 54 ± 2 cells/mm^2, 78 ± 3% Sham, $q = 6.192$, $P < 0.01$; 6 weeks: 51 ± 2 cells/mm^2, 75 ± 4% Sham, $q = 6.329$, $P < 0.01$).

Consequently, the ratio (Fig. 8B) of perilesional:contralesional cortex displayed an early and sustained Otx2 imbalance across hemispheres, which preceded PV+ cell loss (compared with Fig. 2B). Double-immunostaining of Otx2 and PV further revealed that the accumulation of Otx2 in PV+ cells was significantly impaired post-TBI in the perilesional cortex ($F_{5,54} = 26.66$, $P < 0.0001$) but not on the contralesional side ($F_{5,54} = 1.552$, $P = 0.1894$). Post hoc analysis indicated that the percentage of PV+ cells containing Otx2 was reduced in the perilesional cortex at 2 weeks ($q = 10.59$, $P < 0.001$) and 4 weeks ($q = 9.048$, $P < 0.001$) after TBI (Fig. 9).

Discussion

We demonstrate for the first time that progressive functional loss of cortical inhibition correlates positively with progressive disruption of cortical inhibitory interneurons following TBI in rats. Importantly, we identified convergent molecular changes related to PV+ cells, the major inhibitory network in the cortex. This sequence provides insights for novel therapeutic strategies during the critical subacute posttraumatic period where pathologic shifts in the *E*:*I* ratio likely begin, yet where biomarkers to detect such change are lacking.

Our study first highlights the sensitivity of LI-ppTMS in monitoring the level of cortical inhibition early after TBI, before clinical sequelae such as PTE are evident, suggesting its translational potential to detect inhibitory deficits in humans after brain injury. In contrast to other TMS protocols which might modulate cortical excitability (Mix et al. 2010; Benali et al. 2011), we demonstrated that repeated exposure to LI-ppTMS, where relatively few pulses are delivered over time, does not affect cortical excitability, adding to the ppTMS translational value.

Previous attempts to predict PTE and other post-TBI syndromes by methods such as magnetic resonance imaging have been inconclusive (Immonen et al. 2013; Shultz et al. 2013). Neuroimaging techniques to diagnose early stages of progressive TBI sequelae including impaired cognition, affective disorders, and diminished motor control are also lacking (Sundman et al. 2015). In vitro studies in a range of rodent cortical injury models have demonstrated reduced cortical inhibition (Mittmann et al. 1994; Schiene et al. 1996; Li and Prince 2002), but the trajectory of inhibitory functional loss and the underlying cellular mechanism in vivo remains largely unknown.

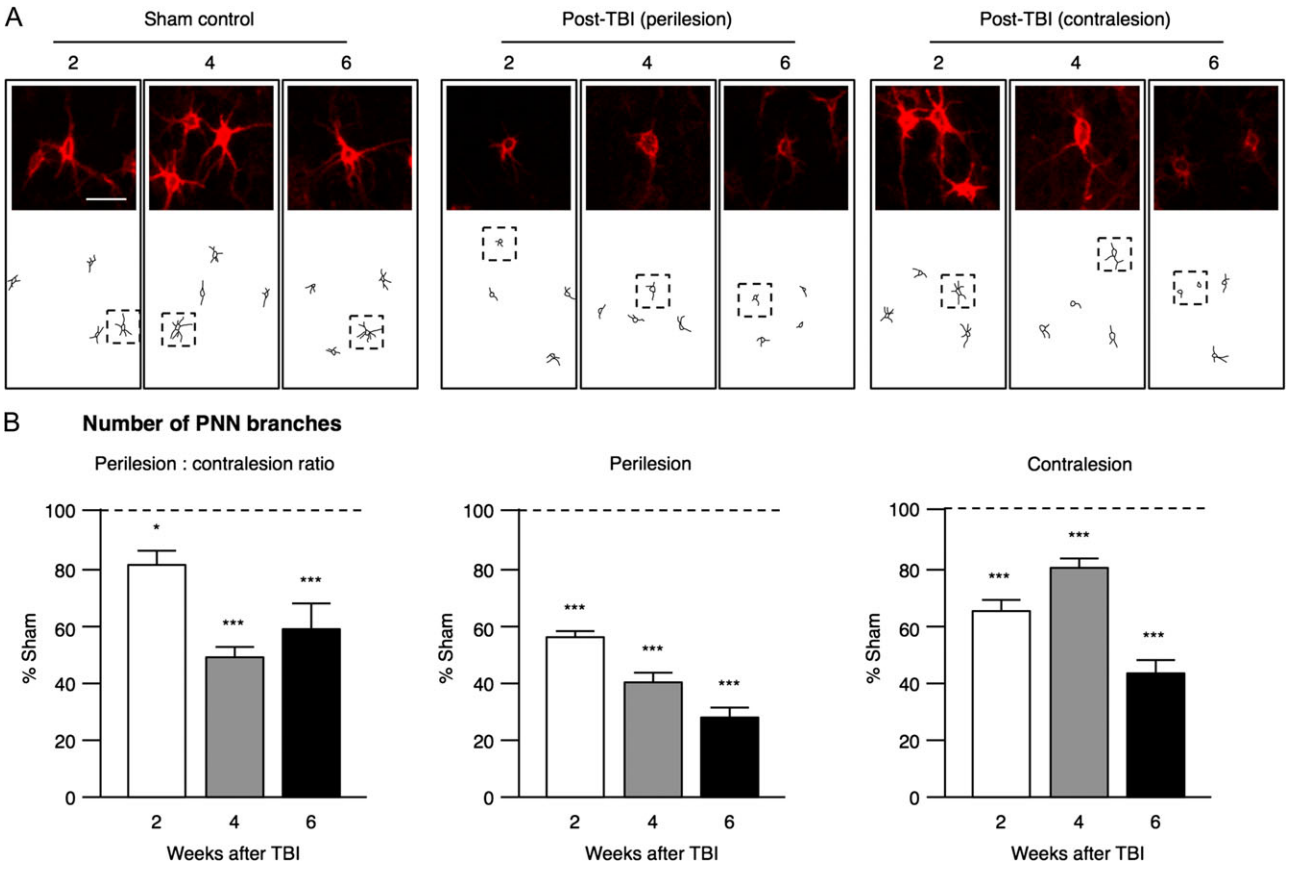

Figure 6. Reduced PNN complexity after TBI. (*A*) Tracings of PNN branches in layer V/VI stained by WFA revealing impoverished structures after TBI. High magnification images of individual PNN+ cells are shown (corresponding to those cells highlighted in the sketch tracing). Scale bar = 25 μm. (*B*) The number of PNN branches at the perilesional side (middle panel), contralesional side (right panel), and their ratio (left panel) calculated for each time point after TBI (2, 4, and 6 weeks) (error bars = SEM, n.s. = not significant, $^{*}P < 0.05$, $^{***}P < 0.001$, Tukey's multiple comparison test, $N = 5$ per group).

To address this unmet need, we demonstrate that significant loss of cortical inhibition is detectable by LI-ppTMS early after injury. This is, for instance, well in advance of the post-traumatic seizures that typically start 6–12 weeks after injury in the rat FPI model (Goodrich et al. 2013; Shultz et al. 2013). Importantly, this loss of inhibition was progressive from the time of injury, which is in agreement with previous studies indicating an increase in the *E:I* ratio as a salient post-TBI consequence (Avramescu et al. 2009; Pitkanen et al. 2009; Hunt et al. 2013; Cantu et al. 2015; Guerriero et al. 2015). LI-ppTMS is non-invasive and can be applied safely to humans (Rotenberg 2010) with close correspondence to findings in rodents (Vahabzadeh-Hagh et al. 2011; Hsieh et al. 2012), suggesting its utility as a practical biomarker for TBI disorders, capable of identifying patients at-risk for PTE and similar syndromes referable to lost cortical inhibition after TBI.

We obtained essentially identical results with LI-ppTMS ISIs of 100 and 200 ms, indicating that potentially a broad range of LI-ppTMS settings (which vary from laboratory to laboratory) may be used to detect compromised cortical inhibition in the subacute post-TBI time window. Importantly 6 weeks after TBI, we also found that successive, weekly application of LI-ppTMS did not cause potentiation or depression of cortical excitability when compared with single LI-ppTMS delivered only once, highlighting that LI-ppTMS might be applied serially to closely monitor the trajectory of patient conditions without changing cortical excitability.

For example, one can test whether ppTMS metrics predict post-traumatic seizures in individual animals (D'Ambrosio et al. 2009) to establish ppTMS as a biomarker for epileptogenesis. Furthermore, ppTMS might be useful in identifying whether an intervention preserves cortical inhibition, predicting efficacy of possible prophylaxis for post-TBI symptoms. Recently, gamma (γ)-oscillations preceding interictal epileptiform spikes have been associated with seizure onset zone in patients with temporal lobe epilepsy (Ren et al. 2015). It would be interesting to determine whether such γ-oscillations monitored by electroencephalography (EEG) might corroborate ppTMS measures. Future studies might then focus on the spatial effect across cortex (beyond motor areas) or subcortical structures, which would be possible with ultrasensitive imaging (Chen et al. 2013) and EEG techniques (Szaflarski et al. 2010).

A limitation of our study is that we did not monitor the rats for clinical post-TBI symptoms, and instead focused on metrics of cortical inhibition. Yet, we selected a model whose clinical consequences from cognitive dysfunction to PTE are well described by our group and others (McIntosh et al. 1996; D'Ambrosio et al. 2005; Bolkvadze and Pitkanen 2012; Goodrich et al. 2013). Future studies may characterize how the loss of cortical inhibition as measured by ppTMS correlates with the range of clinical consequences that follow TBI. Here, we instead aimed to identify a mechanism that might explain the multitude of clinical consequences of TBI.

Our ppTMS findings of a functional loss of $GABA_A$-mediated inhibition post-TBI prompted histological analysis of GABAergic interneurons. Among this heterogeneous population (Ascoli et al. 2008), PV+ cells are of particular interest for

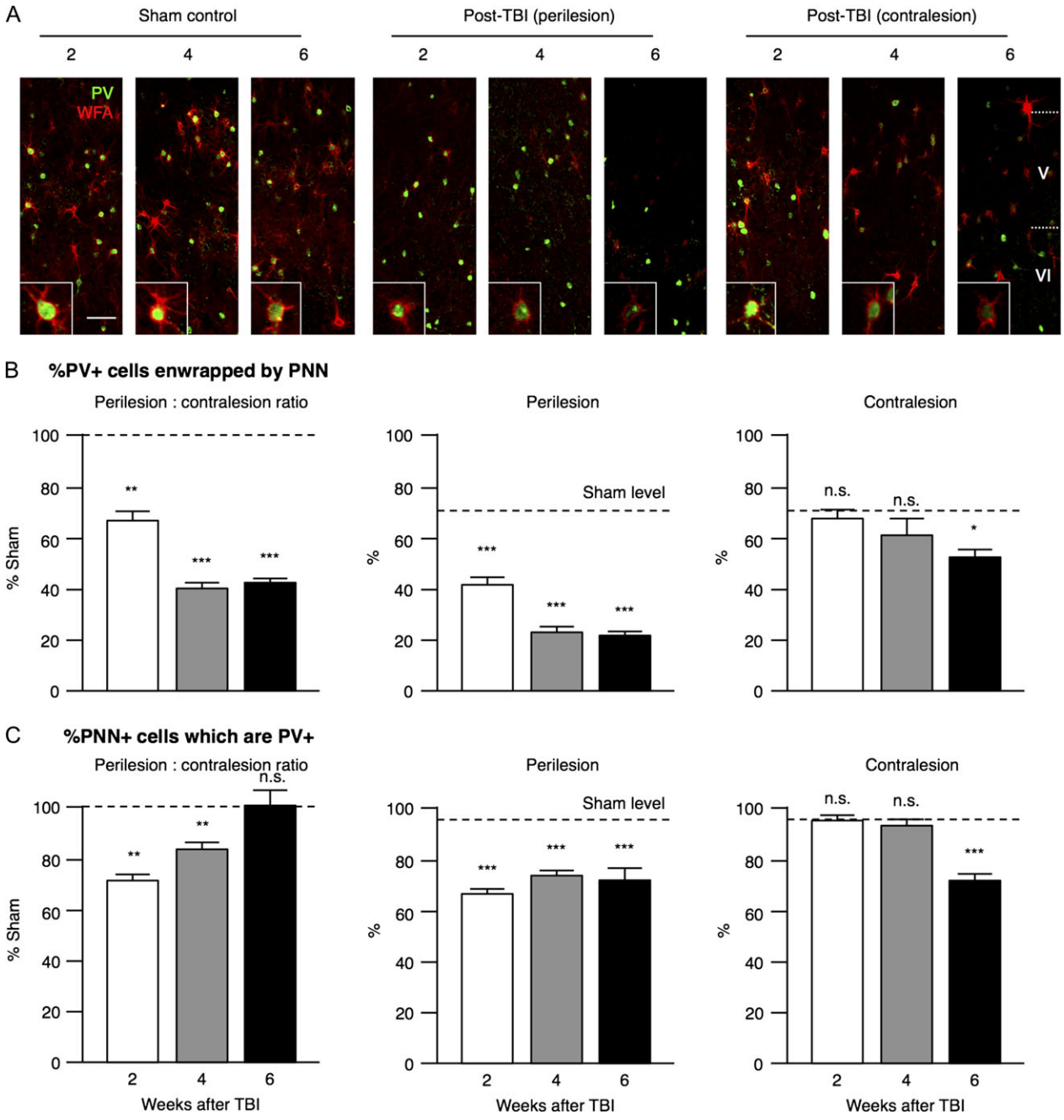

Figure 7. Loss of PV+ cells enwrapped by PNN after TBI. (*A*) Rats underwent sham operation (Sham) or FPI (post-TBI) then sacrificed at different time points (2, 4, and 6 weeks). Cortical sections through motor area were stained with anti-PV (shown in green) and WFA (shown in red). Confocal images (600 × 400 μm) from Sham control, perilesional and contralesional sides from post-TBI brains are shown. Scale bar = 100 μm. High magnification images of individual cells are displayed in insets. (*B*) Percentage of PV+ cells positively stained with WFA at the perilesional side (middle panel), contralesional side (right panel), and their ratio (left panel) calculated for each time point after TBI (2, 4, and 6 weeks). (*C*) Loss of PNN+ cells which are PV+ after TBI. The percentage of PNN+ cells positively stained with PV at the perilesional side (middle panel), contralesional side (right panel), and their ratio (left panel) calculated for each time point after TBI (2, 4, and 6 weeks). Results are compared with sham levels as indicated by the dotted line (error bars = SEM, n.s. = not significant, $^{*}P < 0.05$, $^{**}P < 0.01$, $^{***}P < 0.001$, Tukey's multiple comparison test, $N = 5$ per group).

several reasons. First, cortical PV+ cells constitute the majority of interneurons that mediate perisomatic inhibition of glutamatergic pyramidal cells (Rudy et al. 2011; Kelsom and Lu 2013). Second, fast-spiking PV+ cells are highly metabolically active and vulnerable to oxidative stress (Cabungcal et al. 2013b) which follows TBI (Awasthi et al. 1997; Lewen et al. 2001; Petronilho et al. 2010). This offers a mechanistic linkage between TBI and impaired cortical inhibition. Third, recruitment of PV+ cells into the hyper-excitable network in vitro is reduced after focal lesions in the cortex (Imbrosci et al. 2014). To further investigate the underlying mechanisms, we thus turned to interneuron biology.

We observed a post-TBI loss of PV staining without significant neuronal death in perilesional regions, as supported by

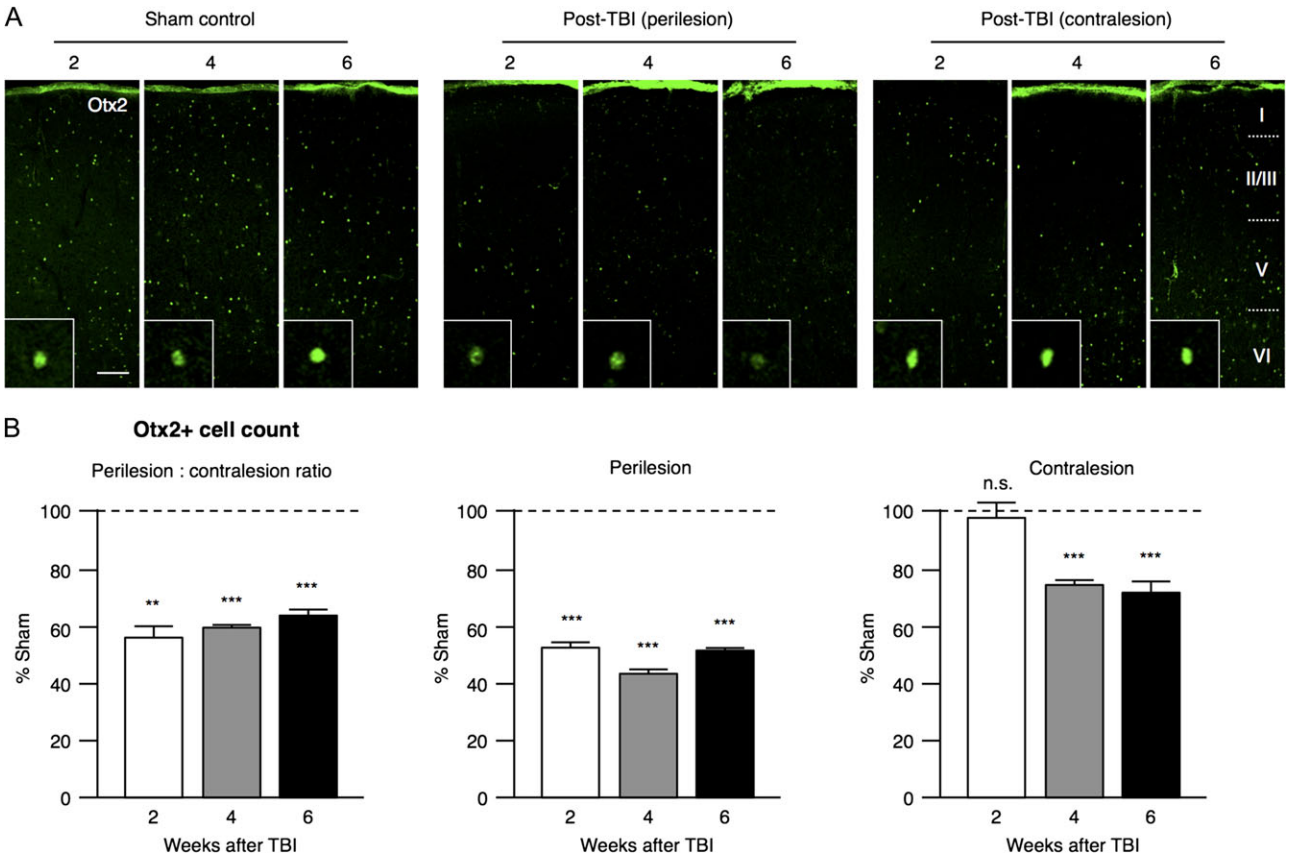

Figure 8. Loss of Otx2 accumulation after TBI. (*A*) Rats underwent sham operation (Sham) or FPI (post-TBI) then sacrificed at different time points (2, 4, and 6 weeks). Cortical sections through motor area were stained with anti-Otx2 (c/o Dr Alain Prochiantz, College de France). Confocal images (900 × 400 μm) from Sham control, perilesional and contralesional sides from post-TBI brains are shown. Cortical layers I–VI are indicated. Scale bar = 100 μm. High magnification images of individual cells are displayed in insets. (*B*) The number of cells positively stained with Otx2 at the perilesional side (middle panel), contralesional side (right panel), and their ratio (left panel) calculated for each time point after TBI (2, 4, and 6 weeks) (error bars = SEM, n.s. = not significant, $^{**}P < 0.01$, $^{***}P < 0.001$, Tukey's multiple comparison test, $N = 5$ per group).

unaltered NeuN staining. In more detail, we found an increasing fraction of PNN+ cells that did not express PV (see Fig. 7). Given that PNNs tightly envelop healthy PV+ cells, one might conclude that PV protein is simply lost after TBI. Yet, our ppTMS data revealed a parallel functional loss of cortical inhibition (Fig 1). Thus, we consider below the possibility of a causal relationship to actual PV+ cell loss of function based on the sequence of post-TBI changes identified here.

Weakening PV signals mirrored a progressive but delayed increase in oxidative stress levels after FPI (Hunt et al. 2013). Previous studies had focused on hours to days after injury, but failed to report redox changes across the longer timeframe of weeks to months as shown here (Awasthi et al. 1997; Lewen et al. 2001; Petronilho et al. 2010). We propose that this sustained posttraumatic increase in oxidative stress is due to the earlier degeneration of the PNNs (Cabungcal et al. 2013a). Compromised PNNs are associated with redox dysregulation in interneurons (Morishita et al. 2015) and local circuit reorganization after spinal cord injury (Orlando and Raineteau 2014). We found PNN integrity to be preferentially compromised in the perilesional cortex, resulting in a decreased number of PV+ cells that are enwrapped (Fig. 7B). This could render them vulnerable to oxidative stress, resulting in eventual cell loss (Fig. 2B).

The expression of CSPG, a major component of the PNN, is also reduced after TBI (Harris et al. 2009). One of these, aggrecan, is degraded by collagenase 3 (encoded by the MMP13 gene, a member of the matrix metallopeptidase (MMP) family) (Fosang et al. 1996). In a model of brain injury induced by focal cerebral ischemia, MMP13 expression increases leading to loss of PNN integrity days after injury (Nagel et al. 2005). MMP-mediated aggrecan proteolysis is also implicated in seizure susceptibility after status epilepticus (Rankin-Gee et al. 2015). Even the sulfation pattern of CSPG is altered in a controlled cortical impact TBI mouse model (Yi et al. 2012), suggesting other post-translational PNN modifications play a role in post-TBI pathophysiology (Fawcett 2015). Our observations of both a declining number of PNN+ cells (Beurdeley et al. 2012) and PNN complexity (Carulli et al. 2010) are consistent with these previous results linking PNN integrity to PV+ cell survival.

Interestingly, our focal, unilateral FPI to the cortex also yielded a contralesional interneuron loss 6 weeks after TBI. Previous studies have reported distal changes after head trauma in subcortical hippocampus (Santhakumar et al. 2001) and thalamus (Huusko and Pitkanen 2014), where region-specific factors such as cytoskeletal composition might play a role in their injury response (de Haas Ratzliff and Soltesz 2000). However, global posttraumatic changes in the neocortex have not been studied longitudinally before (Cantu et al. 2015). Possible mechanisms for such long-range, delayed impact found in contralesional sites include 1) contrecoup injury (Cepeda et al. 2015); 2) epileptiform activity that spreads across

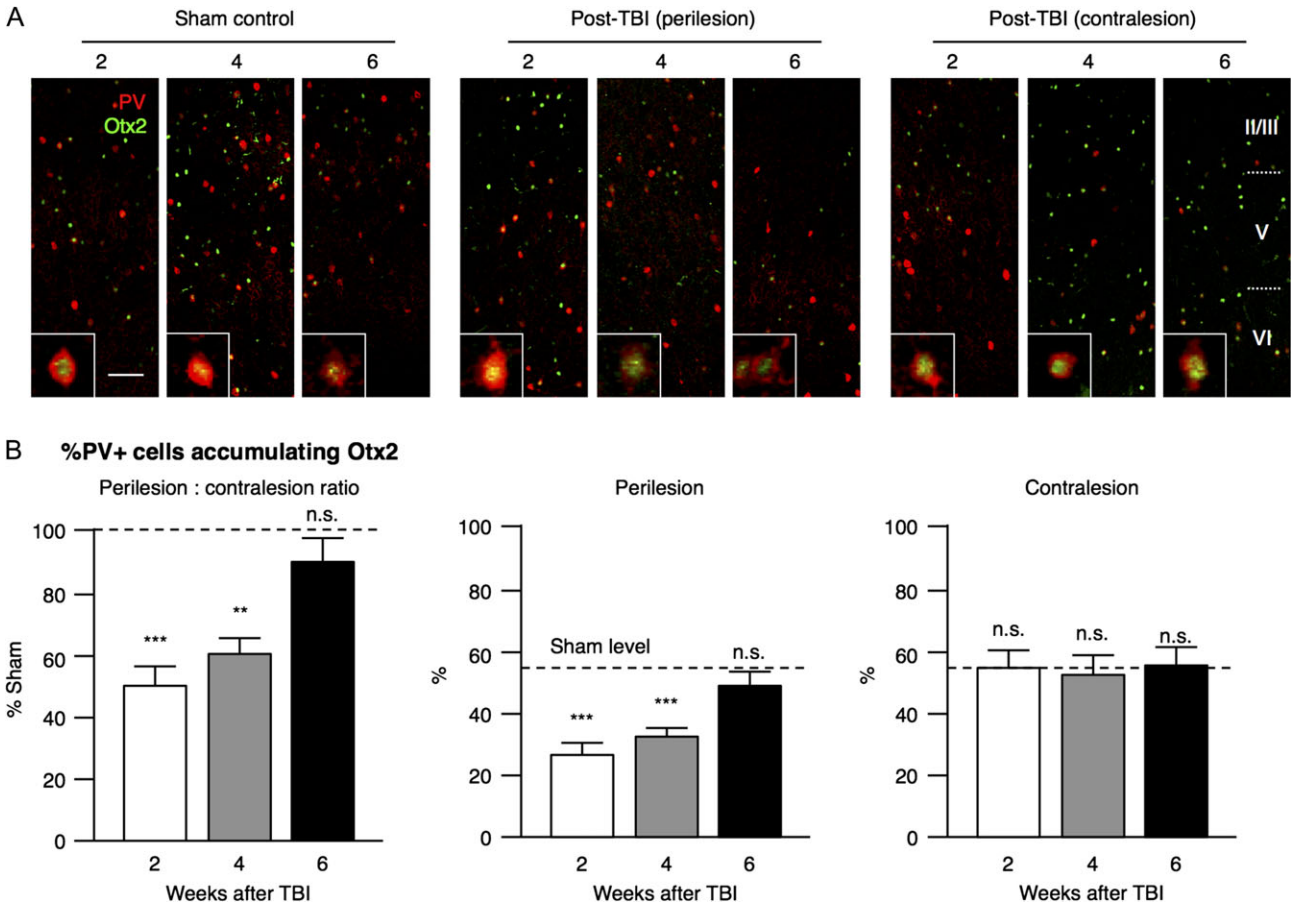

Figure 9. Retention of PV+ cells accumulating Otx2 after TBI. (*A*) Rats underwent sham operation (Sham) or FPI (post-TBI) then sacrificed at different time points (2, 4, and 6 weeks). Cortical sections through motor area were stained with anti-PV (shown in red) and anti-Otx2 (shown in green). Confocal images (600 × 400 μm) from Sham control, perilesional and contralesional sides from post-TBI brains are shown. Scale bar = 100 μm. High magnification images of individual cells are displayed in insets. (*B*) Percentage of PV+ cells positively stained with Otx2 at the perilesional side (middle panel), contralesional side (right panel), and their ratio (left panel) calculated for each time point after TBI (2, 4, and 6 weeks). Results are compared with sham levels as indicated by the dotted line (error bars = SEM, n.s. = not significant, $^{*}P < 0.05$, $^{**}P < 0.01$, $^{***}P < 0.001$; Tukey's multiple comparison test, $N = 5$ per group).

hemispheres by subcortical (Pitkanen et al. 2009) or callosal connections (Laitinen et al. 2015); or 3) a loss of Otx2 production from the choroid plexus (Spatazza et al. 2013) which could result from the initial injury (Makino 2004). Whether and to what extent each of these mechanisms contributes to distal post-TBI cortical changes can be investigated in future studies where the pathologic extent and change over time is more completely characterized in the lesional and contralesional hemisphere.

Accumulation of the homeoprotein Otx2 in PV+ cells is critical for PNN maintenance in mice (Beurdeley et al. 2012). Here, we find that the level of Otx2 was rapidly reduced post-TBI in rats (Fig. 8*B*), mirroring the rapid decline in PNN integrity (Figs 5 and 6). Conversely, the percentage of remaining PV+ cells co-expressing Otx2 gradually increased after injury (Fig. 9*B*), indicating their dependence on this factor for survival. The choroid plexus is a major source of Otx2 which diffuses broadly through the parenchyma in the adult brain to maintain PV+ circuit function and stability (Beurdeley et al. 2012; Spatazza et al. 2013). We speculate that secondary consequences of TBI, such as impaired ventricular function (Makino 2004) or posttraumatic hydrocephalus in our model (Hameed et al. 2014), might lead to a reduced global Otx2 supply. This in turn could explain even the late, contralesional loss of Otx2 and PNN after TBI.

Given the highly conserved Otx2 sequence homology across species, particularly its PNN-binding motifs (100% identical across mice, rats, and humans; GenBank), we speculate that Otx2 might regulate PV+ cell viability and function through a similar fashion across species. Interestingly, human PNN deficits have been heavily implicated in neurological disorders including epilepsy (Berezin et al. 2014), saccadic palsy (Eggers et al. 2015), amblyopia (Soleman et al. 2013), impaired cognition and dementia (Morawski et al. 2014), some of which are also TBI sequelae. Given that the PNN is a promising therapeutic target in functional recovery after stroke (Gherardini et al. 2015) or amblyopia after reverse eye-patching (Soleman et al. 2013), our findings suggest the PNN as a therapeutic target in the management of post-TBI symptoms.

Since homeoproteins may be neuroprotective (Joshi et al. 2011), we believe an exogenous supply of Otx2 protein could be beneficial for managing post-TBI symptoms, like prevention of PTE during this critical period. In particular, the Otx2 signal derived from the choroid plexus is accessible from the blood periphery, which might overcome some of the technical challenges of targeting PV+ interneurons in the human brain (Sebe and Baraban 2011). Alternatively, emerging evidence supports clearance of reactive oxygen species as a therapeutic approach to protect PV+ cells post-TBI. Powerful antioxidants,

N-acetylcysteine (NAC) or its more brain permeable version NACamide (Pandya et al. 2014), may prove useful as an acute treatment for mild TBI in combat zones (Hoffer et al. 2013). Notably, NAC is approved by the US Food and Drug Administration (FDA), accelerating translational exploration of its efficacy in posttraumatic anti-epileptogenesis and related syndromes.

In summary, we show for the first time an impairment of specific interneurons in the neocortex concomitant with gradual weakening of cortical inhibition consequent to TBI in vivo. Build-up of oxidative stress after an earlier loss of PNNs and Otx2 provide an underlying mechanism for the posttraumatic PV+ cell disruption, which likely contributes to TBI sequelae such as PTE. Functionally, LI-ppTMS detects this trajectory of weakening cortical inhibition. Since non-invasive ppTMS is available to humans, our findings can be readily translated to head trauma patients for the prognosis of posttraumatic symptoms. While beyond the scope of this study, we anticipate therapeutic intervention strategies post-TBI to include well-timed Otx2 enhancement or antioxidant supplementation, which can now be monitored by ppTMS during recovery.

Author's contributions

T.H.H., H.H.C.L., T.K.H., and A.R. designed experiments. T.H.H. carried out TBI and LI-ppTMS experiments. H.H.C.L. carried out immunohistochemistry. M.Q.H. carried out TBI. T.K.H., A.P.L., and A.R. provided equipment and reagents. T.H.H., H.H.C.L., M. Q.H., A.P.L., T.K.H., and A.R. contributed to writing and editing of the manuscript.

Supplementary Material

Supplementary material can be found at: http://www.cercor.oxfordjournals.org/.

Funding

Boston Children's Hospital Translational Research Program (A.R. and T.K.H.), NIH National Institute of Neurological Disorders and Stroke (NINDS) R01 NS088583 (A.R. and T.K.H.), the Assimon Family Fund (A.R.), the Ministry of Science and Technology of Taiwan (MOST 103-2320-B-182-033-MY2, MOST 105-2314-B-182-016) and Chang Gung Memorial Hospital (CMRPD1F0501) to T.H.H.. H.H.C.L. was further supported by a postdoctoral fellowship from the Croucher Foundation (Hong Kong) and funding from the Georgetown University Center for Brain Plasticity and Recovery (to T.K.H.).

Notes

We thank Drs Alain Prochiantz (College de France) for the gift of Otx2 antibody, and Nathaniel Hodgson for critical comments on the manuscript. *Conflicts of Interest*: T.H.H., H.H.C.L., and M.Q. H. have nothing to declare. A.R. is a cofounder and consults for Neuro'motion Inc., consults for NeuroRex Inc., and a coinventor of a patent for real-time integration of TMS and EEG A.R. receives or has received research funding from Sage, Eisai, Neuropace, Neuroelectrics, and Brainsway. A.P.L. has consulted for Nexstim, Neuronix, Starlab Neuroscience, Neuroelectrics, Magstim, Neosync, and Axilum Robotics, and is a coinventor of a patent for real-time integration of TMS, EEG, and MRI T.K.H. receives funding from Pfizer to work on oxidative stress in schizophrenia models. None of the aforementioned relationships conflict with the current experiments.

References

Andary MT, Crewe N, Ganzel SK, Haines-Pepi C, Kulkarni MR, Stanton DF, Thompson A, Yosef M. 1997. Traumatic brain injury/chronic pain syndrome: a case comparison study. Clin J Pain. 13:244–250.

Andre V, Marescaux C, Nehlig A, Fritschy JM. 2001. Alterations of hippocampal GABAergic system contribute to development of spontaneous recurrent seizures in the rat lithium-pilocarpine model of temporal lobe epilepsy. Hippocampus. 11:452–468.

Ascoli GA, Alonso-Nanclares L, Anderson SA, Barrionuevo G, Benavides-Piccione R, Burkhalter A, Buzsaki G, Cauli B, Defelipe J, Fairen A, et al. 2008. Petilla terminology: nomenclature of features of GABAergic interneurons of the cerebral cortex. Nat Rev Neurosci. 9:557–568.

Avramescu S, Nita DA, Timofeev I. 2009. Neocortical post-traumatic epileptogenesis is associated with loss of GABAergic neurons. J Neurotrauma. 26:799–812.

Awasthi D, Church DF, Torbati D, Carey ME, Pryor WA. 1997. Oxidative stress following traumatic brain injury in rats. Surg Neurol. 47:575–581.

Badawy RA, Strigaro G, Cantello R. 2014. TMS, cortical excitability and epilepsy: the clinical impact. Epilepsy Res. 108:153–161.

Barker AT, Dixon RA, Sharrard WJ, Sutcliffe ML. 1984. Pulsed magnetic field therapy for tibial non-union. Interim results of a double-blind trial. Lancet. 1:994–996.

Bashir S, Vernet M, Yoo WK, Mizrahi I, Theoret H, Pascual-Leone A. 2012. Changes in cortical plasticity after mild traumatic brain injury.. Restor Neurol Neurosci. 30:277–282.

Benali A, Trippe J, Weiler E, Mix A, Petrasch-Parwez E, Girzalsky W, Eysel UT, Erdmann R, Funke K. 2011. Theta-burst transcranial magnetic stimulation alters cortical inhibition. J Neurosci. 31:1193–1203.

Berezin V, Walmod PS, Filippov M, Dityatev A. 2014. Targeting of ECM molecules and their metabolizing enzymes and receptors for the treatment of CNS diseases. Prog Brain Res. 214:353–388.

Beurdeley M, Spatazza J, Lee HH, Sugiyama S, Bernard C, Di Nardo AA, Hensch TK, Prochiantz A. 2012. Otx2 binding to perineuronal nets persistently regulates plasticity in the mature visual cortex. J Neurosci. 32:9429–9437.

Bolkvadze T, Pitkanen A. 2012. Development of post-traumatic epilepsy after controlled cortical impact and lateral fluid-percussion-induced brain injury in the mouse. J Neurotrauma. 29:789–812.

Cabungcal JH, Steullet P, Kraftsik R, Cuenod M, Do KQ. 2013a. Early-life insults impair parvalbumin interneurons via oxidative stress: reversal by N-acetylcysteine. Biol Psychiatry. 73:574–582.

Cabungcal JH, Steullet P, Morishita H, Kraftsik R, Cuenod M, Hensch TK, Do KQ. 2013b. Perineuronal nets protect fast-spiking interneurons against oxidative stress. Proc Natl Acad Sci U S A. 110:9130–9135.

Cantu D, Walker K, Andresen L, Taylor-Weiner A, Hampton D, Tesco G, Dulla CG. 2015. Traumatic brain injury increases cortical glutamate network activity by compromising GABAergic control. Cereb Cortex. 25:2306–2320.

Carulli D, Pizzorusso T, Kwok JC, Putignano E, Poli A, Forostyak S, Andrews MR, Deepa SS, Glant TT, Fawcett JW. 2010.

Animals lacking link protein have attenuated perineuronal nets and persistent plasticity. Brain. 133:2331–2347.
Carulli D, Rhodes KE, Fawcett JW. 2007. Upregulation of aggrecan, link protein 1, and hyaluronan synthases during formation of perineuronal nets in the rat cerebellum. J Comp Neurol. 501:83–94.
Cepeda S, Gomez PA, Castano-Leon AM, Munarriz PM, Paredes I, Lagares A. 2015. Contrecoup traumatic intracerebral hemorrhage: a geometric study of the impact site and association with hemorrhagic progression. J Neurotrauma. 33:1034–46.
Chen TW, Wardill TJ, Sun Y, Pulver SR, Renninger SL, Baohan A, Schreiter ER, Kerr RA, Orger MB, Jayaraman V, et al. 2013. Ultrasensitive fluorescent proteins for imaging neuronal activity. Nature. 499:295–300.
D'Ambrosio R, Fender JS, Fairbanks JP, Simon EA, Born DE, Doyle DL, Miller JW. 2005. Progression from frontal-parietal to mesial-temporal epilepsy after fluid percussion injury in the rat. Brain. 128:174–188.
D'Ambrosio R, Hakimian S, Stewart T, Verley DR, Fender JS, Eastman CL, Sheerin AH, Gupta P, Diaz-Arrastia R, Ojemann J, et al. 2009. Functional definition of seizure provides new insight into post-traumatic epileptogenesis. Brain. 132: 2805–2821.
de Haas Ratzliff A, Soltesz I. 2000. Differential expression of cytoskeletal proteins in the dendrites of parvalbumin-positive interneurons versus granule cells in the adult rat dentate gyrus. Hippocampus. 10:162–168.
Eggers SD, Horn AK, Roeber S, Hartig W, Nair G, Reich DS, Leigh RJ. 2015. Saccadic palsy following cardiac surgery: possible role of perineuronal nets. PloS One. 10:e0132075.
Fawcett JW. 2015. The extracellular matrix in plasticity and regeneration after CNS injury and neurodegenerative disease. Prog Brain Res. 218:213–226.
Fosang AJ, Last K, Knauper V, Murphy G, Neame PJ. 1996. Degradation of cartilage aggrecan by collagenase-3 (MMP-13). FEBS Lett. 380:17–20.
Fraser DD, Morrison G. 2009. Brain oxidative stress after traumatic brain injury .. cool it? Crit Care Med. 37:787–788.
Gherardini L, Gennaro M, Pizzorusso T. 2015. Perilesional treatment with chondroitinase ABC and motor training promote functional recovery after stroke in rats. Cereb Cortex. 25(1): 202–212.
Golarai G, Greenwood AC, Feeney DM, Connor JA. 2001. Physiological and structural evidence for hippocampal involvement in persistent seizure susceptibility after traumatic brain injury. J Neurosci. 21:8523–8537.
Goodrich GS, Kabakov AY, Hameed MQ, Dhamne SC, Rosenberg PA, Rotenberg A. 2013. Ceftriaxone treatment after traumatic brain injury restores expression of the glutamate transporter, GLT-1, reduces regional gliosis, and reduces post-traumatic seizures in the rat. J Neurotrauma. 30:1434–1441.
Greve MW, Zink BJ. 2009. Pathophysiology of traumatic brain injury. Mt Sinai J Med. 76:97–104.
Guerriero RM, Giza CC, Rotenberg A. 2015. Glutamate and GABA imbalance following traumatic brain injury. Curr Neurol Neurosci Rep. 15:27.
Hameed MQ, Goodrich GS, Dhamne SC, Amandusson A, Hsieh TH, Mou D, Wang Y, Rotenberg A. 2014. A rapid lateral fluid percussion injury rodent model of traumatic brain injury and post-traumatic epilepsy. Neuroreport. 25:532–536.
Harris NG, Carmichael ST, Hovda DA, Sutton RL. 2009. Traumatic brain injury results in disparate regions of chondroitin sulfate proteoglycan expression that are temporally limited. J Neurosci Res. 87:2937–2950.
Hayes RL, Yang K, Raghupathi R, McIntosh TK. 1995. Changes in gene expression following traumatic brain injury in the rat. J Neurotrauma. 12:779–790.
Hoffer ME, Balaban C, Slade MD, Tsao JW, Hoffer B. 2013. Amelioration of acute sequelae of blast induced mild traumatic brain injury by N-acetyl cysteine: a double-blind, placebo controlled study. PloS One. 8:e54163.
Hou L, Han X, Sheng P, Tong W, Li Z, Xu D, Yu M, Huang L, Zhao Z, Lu Y, et al. 2013. Risk factors associated with sleep disturbance following traumatic brain injury: clinical findings and questionnaire based study. PloS One. 8:e76087.
Hsieh TH, Dhamne SC, Chen JJ, Pascual-Leone A, Jensen FE, Rotenberg A. 2012. A new measure of cortical inhibition by mechanomyography and paired-pulse transcranial magnetic stimulation in unanesthetized rats. J Neurophysiol. 107:966–972.
Hunt RF, Boychuk JA, Smith BN. 2013. Neural circuit mechanisms of post-traumatic epilepsy. Front Cell Neurosci. 7:89.
Huusko N, Pitkanen A. 2014. Parvalbumin immunoreactivity and expression of GABAA receptor subunits in the thalamus after experimental TBI. Neuroscience. 267:30–45.
Imbrosci B, Neitz A, Mittmann T. 2014. Focal cortical lesions induce bidirectional changes in the excitability of fast spiking and non fast spiking cortical interneurons. PloS One. 9: e111105.
Immonen R, Kharatishvili I, Grohn O, Pitkanen A. 2013. MRI biomarkers for post-traumatic epileptogenesis. J Neurotrauma. 30:1305–1309.
Jensen FE. 2009. Introduction–epileptogenic cortical dysplasia: emerging trends in diagnosis, treatment, and pathogenesis. Epilepsia. 50 (Suppl 9):1–2.
Jorge RE, Acion L, Starkstein SE, Magnotta V. 2007. Hippocampal volume and mood disorders after traumatic brain injury. Biol Psychiatry. 62:332–338.
Jorge RE, Arciniegas DB. 2014. Mood disorders after TBI. Psychiatr Clin North Am. 37:13–29.
Joshi RL, Torero Ibad R, Rheey J, Castagner F, Prochiantz A, Moya KL. 2011. Cell non-autonomous functions of homeoproteins in neuroprotection in the brain. FEBS Lett. 585: 1573–1578.
Kelsom C, Lu W. 2013. Development and specification of GABAergic cortical interneurons. Cell Biosci. 3:19.
Kobayashi M, Pascual-Leone A. 2003. Transcranial magnetic stimulation in neurology. Lancet Neurol. 2:145–156.
Kwok JC, Dick G, Wang D, Fawcett JW. 2011. Extracellular matrix and perineuronal nets in CNS repair. Dev Neurobiol. 71: 1073–1089.
Laitinen T, Bolkvadze T, Pitkanen A, Grohn O. 2015. Diffusion tensor imaging detects chronic microstructural changes in white and gray matter after traumatic brain injury in rat. Frontiers in Neuroscience. 9:128.
Lefebvre G, Tremblay S, Theoret H. 2015. Probing the effects of mild traumatic brain injury with transcranial magnetic stimulation of the primary motor cortex. Brain Injury. 29: 1032–1043.
Lewen A, Fujimura M, Sugawara T, Matz P, Copin JC, Chan PH. 2001. Oxidative stress-dependent release of mitochondrial cytochrome c after traumatic brain injury. J cereb Blood Flow Metab. 21:914–920.
Li H, Prince DA. 2002. Synaptic activity in chronically injured, epileptogenic sensory-motor neocortex. J Neurophysiol. 88:2–12.

Lowenstein DH. 2009. Epilepsy after head injury: an overview. Epilepsia. 50 ((Suppl 2)):4–9.

Lucke-Wold BP, Nguyen L, Turner RC, Logsdon AF, Chen YW, Smith KE, Huber JD, Matsumoto R, Rosen CL, Tucker ES, et al. 2015. Traumatic brain injury and epilepsy: underlying mechanisms leading to seizure. Seizure. 33:13–23.

Major BP, Rogers MA, Pearce AJ. 2015. Using transcranial magnetic stimulation to quantify electrophysiological changes following concussive brain injury: a systematic review. Clin Exp Pharmacol Physiol. 42:394–405.

Makino Y. 2004. Morphological changes of cerebral ventricular wall in traumatic brain injury evaluated via large histological specimens. J Neurotrauma. 21:585–594.

McIntosh TK, Smith DH, Meaney DF, Kotapka MJ, Gennarelli TA, Graham DI. 1996. Neuropathological sequelae of traumatic brain injury: relationship to neurochemical and biomechanical mechanisms. Lab Invest. 74:315–342.

Mittmann T, Luhmann HJ, Schmidt-Kastner R, Eysel UT, Weigel H, Heinemann U. 1994. Lesion-induced transient suppression of inhibitory function in rat neocortex in vitro. Neuroscience. 60:891–906.

Mix A, Benali A, Eysel UT, Funke K. 2010. Continuous and intermittent transcranial magnetic theta burst stimulation modify tactile learning performance and cortical protein expression in the rat differently. Eur J Neurosci. 32: 1575–1586.

Morawski M, Filippov M, Tzinia A, Tsilibary E, Vargova L. 2014. ECM in brain aging and dementia. Prog Brain Res. 214: 207–227.

Morishita H, Cabungcal JH, Chen Y, Do KQ, Hensch TK. 2015. Prolonged period of cortical plasticity upon redox dysregulation in fast-spiking interneurons. Biol Psychiatry. 78:396–402.

Muller PA, Dhamne SC, Vahabzadeh-Hagh AM, Pascual-Leone A, Jensen FE, Rotenberg A. 2014. Suppression of motor cortical excitability in anesthetized rats by low frequency repetitive transcranial magnetic stimulation. PloS One. 9: e91065.

Nagel S, Sandy JD, Meyding-Lamade U, Schwark C, Bartsch JW, Wagner S. 2005. Focal cerebral ischemia induces changes in both MMP-13 and aggrecan around individual neurons. Brain Res. 1056:43–50.

Nampiaparampil DE. 2008. Prevalence of chronic pain after traumatic brain injury: a systematic review. JAMA. 300: 711–719.

Orlando C, Raineteau O. 2014. Integrity of cortical perineuronal nets influences corticospinal tract plasticity after spinal cord injury. Brain Struct Funct. 220:1077–1091.

Pandya JD, Readnower RD, Patel SP, Yonutas HM, Pauly JR, Goldstein GA, Rabchevsky AG, Sullivan PG. 2014. N-acetylcysteine amide confers neuroprotection, improves bioenergetics and behavioral outcome following TBI. Exp Neurol. 257:106–113.

Petronilho F, Feier G, de Souza B, Guglielmi C, Constantino LS, Walz R, Quevedo J, Dal-Pizzol F. 2010. Oxidative stress in brain according to traumatic brain injury intensity. J Surg Res. 164:316–320.

Pitkanen A, Immonen RJ, Grohn OH, Kharatishvili I. 2009. From traumatic brain injury to posttraumatic epilepsy: what animal models tell us about the process and treatment options. Epilepsia. 50 ((Suppl 2)):21–29.

Potts MB, Adwanikar H, Noble-Haeusslein LJ. 2009. Models of traumatic cerebellar injury. Cerebellum. 8:211–221.

Prince DA, Jacobs K. 1998. Inhibitory function in two models of chronic epileptogenesis. Epilepsy Res. 32:83–92.

Prince DA, Parada I, Scalise K, Graber K, Jin X, Shen F. 2009. Epilepsy following cortical injury: cellular and molecular mechanisms as targets for potential prophylaxis. Epilepsia. 50 ((Suppl 2)):30–40.

Rakhade SN, Jensen FE. 2009. Epileptogenesis in the immature brain: emerging mechanisms. Nat Rev Neurol. 5:380–391.

Rankin-Gee EK, McRae PA, Baranov E, Rogers S, Wandrey L, Porter BE. 2015. Perineuronal net degradation in epilepsy. Epilepsia. 56:1124–1133.

Rao V, McCann U, Han D, Bergey A, Smith MT. 2014. Does acute TBI-related sleep disturbance predict subsequent neuropsychiatric disturbances? Brain Inj. 28:20–26.

Ren L, Kucewicz MT, Cimbalnik J, Matsumoto JY, Brinkmann BH, Hu W, Marsh WR, Meyer FB, Stead SM, Worrell GA. 2015. Gamma oscillations precede interictal epileptiform spikes in the seizure onset zone. Neurology. 84:602–608.

Rodgers KM, Bercum FM, McCallum DL, Rudy JW, Frey LC, Johnson KW, Watkins LR, Barth DS. 2012. Acute neuroimmune modulation attenuates the development of anxiety-like freezing behavior in an animal model of traumatic brain injury. J Neurotrauma. 29:1886–1897.

Rodriguez-Rodriguez A, Egea-Guerrero JJ, Murillo-Cabezas F, Carrillo-Vico A. 2014. Oxidative stress in traumatic brain injury. Curr Med Chem. 21:1201–1211.

Rotenberg A. 2010. Prospects for clinical applications of transcranial magnetic stimulation and real-time EEG in epilepsy. Brain Topogr. 22:257–266.

Rowe RK, Harrison JL, O'Hara BF, Lifshitz J. 2014. Recovery of neurological function despite immediate sleep disruption following diffuse brain injury in the mouse: clinical relevance to medically untreated concussion. Sleep. 37:743–752.

Rudy B, Fishell G, Lee S, Hjerling-Leffler J. 2011. Three groups of interneurons account for nearly 100% of neocortical GABAergic neurons. Dev Neurobiol. 71:45–61.

Santhakumar V, Ratzliff AD, Jeng J, Toth Z, Soltesz I. 2001. Long-term hyperexcitability in the hippocampus after experimental head trauma. Ann Neurol. 50:708–717.

Sawyer K, Bell KR, Ehde DM, Temkin N, Dikmen S, Williams RM, Dillworth T, Hoffman JM. 2015. Longitudinal study of headache trajectories in the year after mild traumatic brain injury: relation to posttraumatic stress disorder symptoms. Arch Phys Med Rehabil. 96:2000–2006.

Schiene K, Bruehl C, Zilles K, Qu M, Hagemann G, Kraemer M, Witte OW. 1996. Neuronal hyperexcitability and reduction of GABAA-receptor expression in the surround of cerebral photothrombosis. J J Cereb Blood Flow Metab. 16:906–914.

Sebe JY, Baraban SC. 2011. The promise of an interneuron-based cell therapy for epilepsy. Dev Neurobiol. 71:107–117.

Shultz SR, Bao F, Omana V, Chiu C, Brown A, Cain DP. 2012. Repeated mild lateral fluid percussion brain injury in the rat causes cumulative long-term behavioral impairments, neuroinflammation, and cortical loss in an animal model of repeated concussion. J Neurotrauma. 29:281–294.

Shultz SR, Cardamone L, Liu YR, Hogan RE, Maccotta L, Wright DK, Zheng P, Koe A, Gregoire MC, Williams JP, et al. 2013. Can structural or functional changes following traumatic brain injury in the rat predict epileptic outcome? Epilepsia. 54:1240–1250.

Skopin MD, Kabadi SV, Viechweg SS, Mong JA, Faden AI. 2015. Chronic decrease in wakefulness and disruption of sleep-wake behavior after experimental traumatic brain injury. J Neurotrauma. 32:289–296.

Soleman S, Filippov MA, Dityatev A, Fawcett JW. 2013. Targeting the neural extracellular matrix in neurological disorders. Neuroscience. 253:194–213.

Spatazza J, Lee HH, Di Nardo AA, Tibaldi L, Joliot A, Hensch TK, Prochiantz A. 2013. Choroid-plexus-derived otx2 homeoprotein constrains adult cortical plasticity. Cell Rep. 3: 1815–1823.

Sugiyama S, Prochiantz A, Hensch TK. 2009. From brain formation to plasticity: insights on Otx2 homeoprotein. Dev Growth Differ. 51:369–377.

Sun DA, Deshpande LS, Sombati S, Baranova A, Wilson MS, Hamm RJ, DeLorenzo RJ. 2008. Traumatic brain injury causes a long-lasting calcium (Ca2+)-plateau of elevated intracellular Ca levels and altered Ca2+ homeostatic mechanisms in hippocampal neurons surviving brain injury. Eur J Neurosci. 27:1659–1672.

Sundman M, Doraiswamy PM, Morey RA. 2015. Neuroimaging assessment of early and late neurobiological sequelae of traumatic brain injury: implications for CTE. Front Neurosci. 9:334.

Szaflarski JP, DiFrancesco M, Hirschauer T, Banks C, Privitera MD, Gotman J, Holland SK. 2010. Cortical and subcortical contributions to absence seizure onset examined with EEG/fMRI. Epilepsy Behav. 18:404–413.

Theadom A, Cropley M, Parmar P, Barker-Collo S, Starkey N, Jones K, Feigin VL, Group BR. 2015. Sleep difficulties one year following mild traumatic brain injury in a population-based study. Sleep Med. 16:926–932.

Torbic H, Forni AA, Anger KE, Degrado JR, Greenwood BC. 2013. Use of antiepileptics for seizure prophylaxis after traumatic brain injury. Am J Health Syst Pharm. 70:759–766.

Vahabzadeh-Hagh AM, Muller PA, Gersner R, Zangen A, Rotenberg A. 2012. Translational neuromodulation: approximating human transcranial magnetic stimulation protocols in rats. Neuromodulation. 15:296–305.

Vahabzadeh-Hagh AM, Muller PA, Pascual-Leone A, Jensen FE, Rotenberg A. 2011. Measures of cortical inhibition by paired-pulse transcranial magnetic stimulation in anesthetized rats. J Neurophysiol. 105:615–624.

Valk-Kleibeuker L, Heijenbrok-Kal MH, Ribbers GM. 2014. Mood after moderate and severe traumatic brain injury: a prospective cohort study. PloS One. 9:e87414.

Yi JH, Katagiri Y, Susarla B, Figge D, Symes AJ, Geller HM. 2012. Alterations in sulfated chondroitin glycosaminoglycans following controlled cortical impact injury in mice. J Comp Neurol. 520:3295–3313.

Ziemann U, Reis J, Schwenkreis P, Rosanova M, Strafella A, Badawy R, Muller-Dahlhaus F. 2015. TMS and drugs revisited 2014. Clin Neurophysiol. 126:1847–1868.